Towards Establishing Best Practice in the Analysis of Hydrogen and Deuterium by Atom Probe Tomography

Baptiste Gault, Aparna Saksena, Xavier Sauvage, Paul Bagot, Leonardo S Aota, Jonas Arlt, Lisa T Belkacemi, Torben Boll, Yi-Sheng Chen, Luke Daly, Milos B Djukic, James O Douglas, Maria J Duarte, Peter J Felfer, Richard G Forbes, Jing Fu, Hazel M Gardner, Ryota Gemma, Stephan S A Gerstl, Yilun Gong, Guillaume Hachet, Severin Jakob, Benjamin M Jenkins, Megan E Jones, Heena Khanchandani, Paraskevas Kontis, Mathias Krämer, Markus Kühbach, Ross K W Marceau, David Mayweg, Katie L Moore, Varatharaja Nallathambi, Benedict C Ott, Jonathan D Poplawsky, Ty Prosa, Astrid Pundt, Mainak Saha, Tim M Schwarz, Yuanyuan Shang, Xiao Shen, Maria Vrellou, Yuan Yu, Yujun Zhao,

Downloaded from https://academic.oup.com/mam/advance-article/doi/10.1093/mam/ozae081/7748435 by guest on 10 October 2024

Microscopy and Microanalysis, 2024, **00**, 1–16
https://doi.org/10.1093/mam/ozae081

Microscopy AND Microanalysis

Review Article

Towards Establishing Best Practice in the Analysis of Hydrogen and Deuterium by Atom Probe Tomography

Baptiste Gault[1,2,*], Aparna Saksena[1,*], Xavier Sauvage[3], Paul Bagot[4], Leonardo S. Aota[1], Jonas Arlt[5], Lisa T. Belkacemi[6,7], Torben Boll[8], Yi-Sheng Chen[9,10], Luke Daly[4,9,11], Milos B. Djukic[12], James O. Douglas[2], Maria J. Duarte[1], Peter J. Felfer[13], Richard G. Forbes[14], Jing Fu[15], Hazel M. Gardner[16], Ryota Gemma[17,18], Stephan S. A. Gerstl[19], Yilun Gong[1,4], Guillaume Hachet[1], Severin Jakob[20], Benjamin M. Jenkins[3], Megan E. Jones[21], Heena Khanchandani[22], Paraskevas Kontis[22], Mathias Krämer[1], Markus Kühbach[23], Ross K. W. Marceau[24], David Mayweg[20], Katie L. Moore[25], Varatharaja Nallathambi[1,26], Benedict C. Ott[13], Jonathan D. Poplawsky[27], Ty Prosa[28], Astrid Pundt[29], Mainak Saha[30], Tim M. Schwarz[1], Yuanyuan Shang[31], Xiao Shen[32], Maria Vrellou[33], Yuan Yu[34], Yujun Zhao[35], Huan Zhao[36], and Bowen Zou[32]

[1]*Max-Planck-Institute für Eisenforschung GmbH (now Max Planck Institute for Sustainable Materials), Max-Planck-Straße 1, Düsseldorf 40237, Germany*
[2]*Department of Materials, Imperial College London, Royal School of Mines, Prince Consort Rd, South Kensington, London SW7 2AZ, UK*
[3]*Groupe de Physique des Matériaux, Univ Rouen Normandie, INSA Rouen Normandie, CNRS, UMR6634, Avenue de l'Université, BP12, 76800 Saint-Etienne-du-Rouvray, France*
[4]*Department of Materials, University of Oxford, Parks Road, Oxford OX1 3PH, UK*
[5]*Institute for Materials Physics, University of Göttingen, Friedrich-Hund-Platz 1, Göttingen D-37077, Germany*
[6]*Leibniz-Institute for Materials Engineering-IWT, Badgasteiner Straße 3, Bremen 28359, Germany*
[7]*MAPEX Center for Materials and Processes, Universität Bremen, Bibliothekstraße 1, Bremen 28359, Germany*
[8]*Institute for Applied Materials (IAM-WK) and Karlsruhe Nano Micro Facility (KNMFi), Karlsruhe Institute of Technology (KIT), Hermann-von-Helmholtz-Platz 1, Eggenstein-Leopoldshafen D-76344, Germany*
[9]*Australian Centre for Microscopy and Microanalysis, Madsen Building F09, The University of Sydney, Camperdown, NSW 2006, Australia*
[10]*School of Materials Science and Engineering, Nayang Technological University, 50 Nanyang Avenue, 639798 Singapore*
[11]*School of Geographical and Earth Sciences, University of Glasgow, 8NN University Avenue, Glasgow G12 8QQ, UK*
[12]*Faculty of Mechanical Engineering, University of Belgrade, Kraljice Marije 16, Belgrade 11120, Serbia*
[13]*Department of Materials Science & Engineering, Institute I: General Materials Properties, Friedrich-Alexander-Universität Erlangen-Nürnberg, Martensstrasse 5, Erlangen 91058, Germany*
[14]*Quantum Foundations and Technologies Group, School of Mathematics and Physics, University of Surrey, Guildford, Surrey GU2 7XH, UK*
[15]*Department of Mechanical and Aerospace Engineering, Monash University, 17 College Walk, Clayton, VIC 3168, Australia*
[16]*Materials Science and Engineering, UK Atomic Energy Authority, Culham Campus, Abingdon, Oxfordshire OX14 3DB, UK*
[17]*Department of Applied Chemistry, Tokai University, 4-1-1 Kitakaname, Hiratsuka, Kanagawa 259-1292, Japan*
[18]*Micro/Nano Technology Center, Tokai University, 4-1-1 Kitakaname, Hiratsuka, Kanagawa 259-1292, Japan*
[19]*Scientific Center for Optical and Electron Microscopy, ETH Zurich, Otto-Stern-Weg 3, Zurich 8093, Switzerland*
[20]*Department of Physics, Chalmers University of Technology, Göteborg SE-412 96, Sweden*
[21]*National Nuclear Laboratory, Windscale Laboratory, Sellafield, Seascale, Cumbria CA20 1PG, UK*
[22]*Department of Materials Science and Engineering, Norwegian University of Science and Technology, 325 Kjemiblokk 1 Gløshaugen, Trondheim 7491, Norway*
[23]*Center for the Science of Materials Berlin, Humboldt-Universität zu Berlin, Zum Großen Windkanal 2, 12489 Berlin, Germany*
[24]*Institute for Frontier Materials, Deakin University, Geelong Waurn Ponds Campus, Waurn Ponds, VIC 3216, Australia*
[25]*Department of Materials, University of Manchester, Oxford Road, Manchester M13 9PL, UK*
[26]*Technical Chemistry I and Center for Nanointegration Duisburg-Essen (CENIDE), University of Duisburg-Essen, Universitätsstraße 5, 45141 Essen, Germany*
[27]*Oak Ridge National Laboratory, Center for Nanophase Materials Sciences, 1 Bethel Valley Road, Oak Ridge, TN 37830, USA*
[28]*CAMECA Instruments, Inc., 5470 Nobel Drive, Madison, WI 53711, USA*
[29]*Karlsruhe Institute of Technology KIT, IAM-WK, Kaiserstraße 12, Karlsruhe 36131, Germany*
[30]*Research Centre for Magnetic and Spintronic Materials, National Institute for Materials Science, 1-2-1 Sengen, Tsukuba, Ibaraki 305-0047, Japan*
[31]*Department of Materials Design, Institute of Hydrogen Technology, Helmholtz-Zentrum Hereon GmbH, Geesthacht 21502, Germany*
[32]*Institute of Materials Engineering, University of Kassel, Moenchebergstr.3, Kassel 34125, Germany*
[33]*Institute for Applied Materials, Karlsruhe Institute of Technology, Kaiserstrasse 12, Karlsruhe 76131, Germany*
[34]*Institute of Physics (IA), RWTH Aachen University, Otto-Blumenthal-Straße 18, Aachen 52056, Germany*

Received: May 21, 2024. **Accepted:** August 15, 2024
© The Author(s) 2024. Published by Oxford University Press on behalf of the Microscopy Society of America.
This is an Open Access article distributed under the terms of the Creative Commons Attribution License (https://creativecommons.org/licenses/by/4.0/), which permits unrestricted reuse, distribution, and reproduction in any medium, provided the original work is properly cited.

Downloaded from https://academic.oup.com/mam/advance-article/doi/10.1093/mam/ozae081/7748435 by guest on 10 October 2024

[35]Institute for Materials, Ruhr-Universität Bochum, Universitätsstraße 150, 44801 Bochum, Germany
[36]State Key Laboratory for Mechanical Behavior of Materials, Xi'an Jiaotong University, Xianning West Road, 28#, Xi'an, Shaanxi Province, 710049, China
*Corresponding author: Baptiste Gault, E-mail: b.gault@mpie.de; Aparna Saksena, E-mail: a.saksena@mpie.de

Abstract

As hydrogen is touted as a key player in the decarbonization of modern society, it is critical to enable quantitative hydrogen (H) analysis at high spatial resolution and, if possible, at the atomic scale. H has a known deleterious impact on the mechanical properties (strength, ductility, toughness) of most materials that can hinder their use as part of the infrastructure of a hydrogen-based economy. Enabling H mapping including local hydrogen concentration analyses at specific microstructural features is essential for understanding the multiple ways that H affect the properties of materials including embrittlement mechanisms and their synergies. In addition, spatial mapping and quantification of hydrogen isotopes is essential to accurately predict tritium inventory of future fusion power plants thus ensuring their safe and efficient operation. Atom probe tomography (APT) has the intrinsic capability to detect H and deuterium (D), and in principle the capacity for performing quantitative mapping of H within a material's microstructure. Yet, the accuracy and precision of H analysis by APT remain affected by complex field evaporation behavior and the influence of residual hydrogen from the ultrahigh vacuum chamber that can obscure the signal of H from within the material. The present article reports a summary of discussions at a focused workshop held at the Max-Planck Institute for Sustainable Materials in April 2024. The workshop was organized to pave the way to establishing best practices in reporting APT data for the analysis of H. We first summarize the key aspects of the intricacies of H analysis by APT and then propose a path for better reporting of the relevant data to support interpretation of APT-based H analysis in materials.

Key words: atom probe tomography, deuterium, hydrogen

Introduction

Hydrogen is the smallest and lightest atom, the most abundant, thus making it ubiquitous. Within the microstructure of materials, hydrogen is known to cause a decrease in toughness, ductility, and resistance to crack propagation through an array of possible mechanisms referred to as hydrogen embrittlement (Hirth, 1980; Pundt & Kirchheim, 2006; Sofronis & Robertson, 2006; Robertson et al., 2015; Lynch, 2019). Despite decades of research, there are still many open questions as to the active mechanism(s) and how to identify them, which is a prerequisite to define strategies to circumvent (or delay) hydrogen embrittlement and enhance the durability and sustainability of engineering parts (Bhadeshia, 2016; Djukic et al., 2019). There are numerous other aspects of hydrogen trapping inside materials. For instance, trapped tritium can pose a radiological hazard especially for maintenance and decommissioning, and that trapped tritium can cause inventory issues by reducing the amount of tritium available for use as fuel.

Scanning tunneling microscopes have been used to manipulate and address individual H atoms on semiconducting surfaces (Simmons et al., 2003). However, quantitative H analysis at high spatial resolution, at least sufficient to directly determine the distribution of H across the microstructure of an engineering alloy, remains extremely challenging. These insights are necessary to complement and inform bulk measurements, either from X-ray or neutron scattering or diffraction (Maxelon et al., 2001), Kelvin probe experiments in a permeation configuration (Evers et al., 2013) or thermal-desorption spectroscopy (TDS) (Choo & Lee, 1982; Merzlikin et al., 2015). Secondary-ion mass spectrometry (Aboura & Moore, 2021; Jones et al., 2021), TDS (Suzuki & Takai, 2012) have made forays in this direction for atomic hydrogen distributed across the microstructure, and transmission-electron microscopy (TEM) (Hamm et al., 2019; de Graaf et al., 2020) has been extensively used for studying hydrides. TEM has also been extensively used for investigating the effects of hydrogen deformation mechanisms (Robertson, 2001); however, there is no way to directly image or map H directly using TEM-based methods.

In principle, atom probe tomography (APT) is the only technique that can combine a capacity for direct detection of H with capabilities for nanoscale, three-dimensional mapping (Cerezo et al., 2007; Kelly & Miller, 2007; Gault et al., 2021). The single-particle detector that equips modern APs (Kelly et al., 2004; Da Costa et al., 2005) uses microchannel plates (MCPs) to convert and amplify the signal from the ion impact. The MCPs are operated in a saturated mode that ensures that their efficiency does not depend on the mass or the energy of the incoming ion. The detector can hence detect H^+ ions, and the mass resolution is typically sufficient to distinguish H^+ from $^2H^+$ or D^+ when isotopic labeling is used. There have been numerous reports of using APT to study the nanoscale distribution of H or D in multilayers (Gemma et al., 2007, 2011), steels (Takahashi et al., 2010, 2018; Chen et al., 2017*b*; Chen et al., 2020; McCarroll et al., 2022; Khanchandani et al., 2023; Jakob et al., 2024; Liu et al., 2024), Al-based (López Freixes et al., 2022; Zhao et al., 2022, 2024) and Ti-based (Chang et al., 2018; Joseph et al., 2022) alloys for instance, as well as to study hydrides (Breen et al., 2018; Mouton et al., 2021; Jones et al., 2022; Mayweg et al., 2023) with numerous other examples in metallic and nonmetallic materials (Martin et al., 2016; Tweddle et al., 2019; Shi et al., 2022; Ott et al., 2024) including geological (Daly et al., 2021*a*; Liu et al., 2022) and extraterrestrial materials (Daly et al., 2020; Greer et al., 2020; Daly et al., 2021*b*).

Despite the unique ability to both detect and map H at the atomic scale in three dimensions, the analysis of H by APT appears subject to an extreme sensitivity to experimental details, including the H-loading samples with hydrogen or deuterium, their preparation and handling pre- and post-H-loading, and the parameters used during acquisition and processing of the data (Takahashi et al., 2010, 2018; Gemma et al., 2011, 2009; Chang et al., 2018; Chang et al., 2019*a*, 2019*b*; Breen et al., 2020; Meier et al., 2023; Jakob et al., 2024). The following sections summarize selected aspects of the discussions raised during the workshop. Topics include the challenges associated with analyzing H by APT possible mitigating solutions, and recommendations for best practices for reporting APT data—with an emphasis on H analysis. We finally provide some perspectives on the future of the field.

Challenges of H Analysis by APT

Figure 1 recaps some of the main challenges associated with the analysis of H by APT that were discussed at length over

Downloaded from https://academic.oup.com/mam/advance-article/doi/10.1093/mam/ozae081/7748435 by guest on 10 October 2024

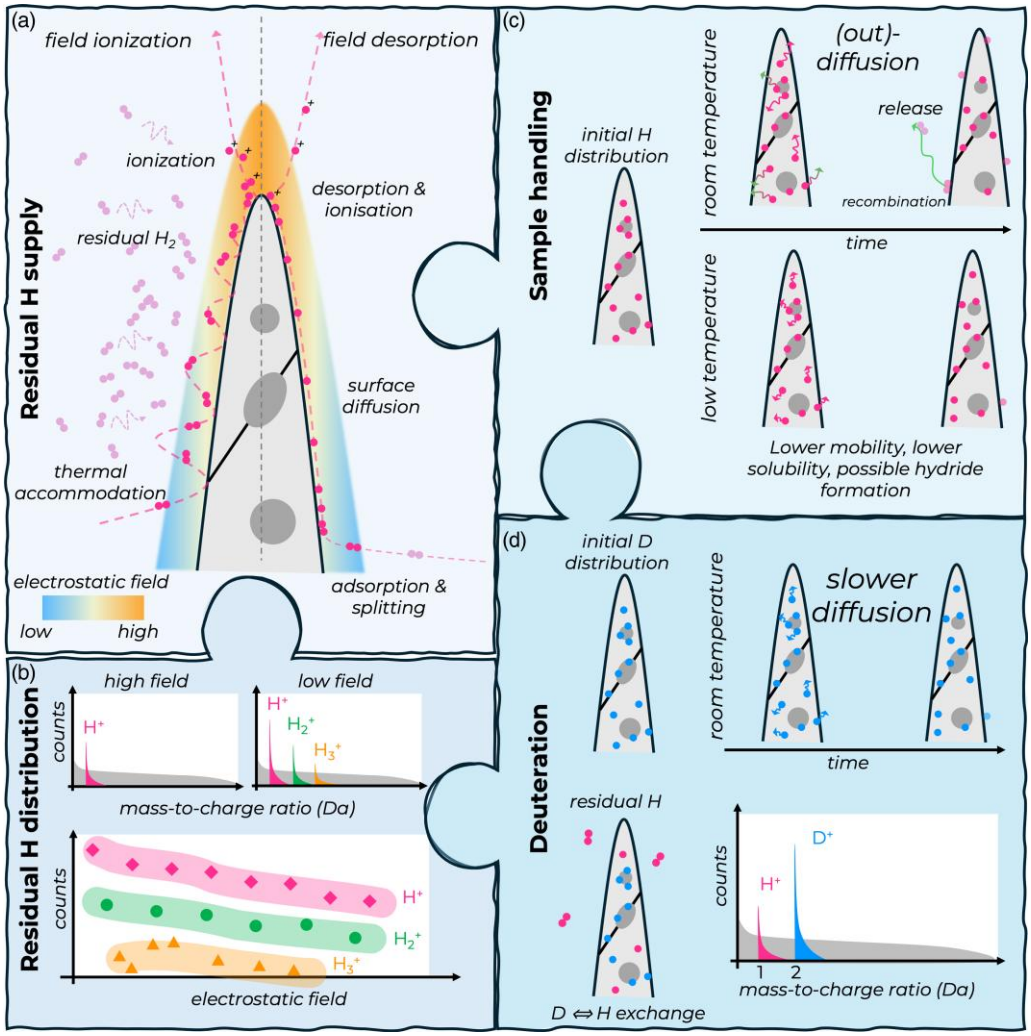

Fig. 1. (**a**) Supply of H to the emitting area at the tip of the specimen from the residual gas; (**b**) electrostatic field dependence on the ionic distribution of H; (**c**) high diffusivity of H that can cause losses from the APT specimen during handling at ambient temperature; (**d**) advantages of deuteration with regards to slower diffusion, and differentiation between H and D in the mass spectrum.

the course of the workshop and are summarized in the following sections. These include the supply function of residual H (A), the dependence of the distribution of H^+, H_2^+, and H_3^+ on the electrostatic field at the specimen apex region (B), the need to control the conditions of temperature and pressure to maintain the H within the microstructure (C), and possible advantages pertaining to the use of deuteration to facilitate the analysis of H by APT (D).

Sources and Behaviors of Residual H

Despite the ultrahigh vacuum level of the analysis chamber, residual H is almost always detected and can obscure the signal from the H ions originating from the specimen of interest. This H comes from the progressive desorption of H_2 from the stainless steel of the chamber walls; it is said that the early atom probe chambers made of glass did not face similar issues. Alternative and promising solutions are being actively pursued to limit the amount of residual H, for instance through the use of chambers and parts made of Ti-based alloys instead of the conventional stainless steel (Felfer et al., 2022). This could be coming in addition to getters or cryo-pumping systems that are more conventionally used.

Once released, gaseous H_2 gets attracted to the cold charged specimen, not unlike the imaging gas dynamics in field-ion microscopy (FIM). The gas supply function in FIM has previously been discussed extensively (Brandon, 1963; Forbes, 1996, 2008). In short, through a series of hops on the surface, the polarized gas atoms or molecules progressively lose energy and thermalize with the surface while moving up the electrostatic field gradient towards the apex region, Figure 1a. As their velocity becomes lower and the electrostatic field higher, the probability for ionization increases with a maximum probability at a so-called critical distance from the surface, as already noted for FIM (Müller & Bahadur, 1956; Forbes, 1996).

An alternative source of residual H is through the formation of an adsorbed layer. Following thermalization, and assisted by the electrostatic field, some of the gas atoms or molecules chemisorb on the surface itself (Rendulic & Knor, 1967). At the surface, H_2 molecules can dissociate into atomic hydrogen. Driven by polarization forces due to the high standing electrostatic field, these atoms or molecules can diffuse along the shank of the specimen towards the apex region (Tsong & Kellogg, 1975). The probability of surface diffusion will hence depend strongly on the nature and energy landscape of the surface (Yoo et al., 2022). Through these mechanisms, H can be

Downloaded from https://academic.oup.com/mam/advance-article/doi/10.1093/mam/ozae081/7748435 by guest on 10 October 2024

continuously supplied to the area being analyzed by APT. This raises the question of whether it would be possible to deposit a material specifically along the specimen's shank that could either slow down or even trap, i.e., getter the H on the specimen shank. This could prevent H from reaching the tip of the specimen where it will eventually be subject to field ion emission and then detected during the experiment.

Upon reaching critical electrostatic fields in the apex region, the probability of field desorption of the adsorbed H becomes sufficiently high to cause the departure of H as either atomic H^+, molecular-ions (i.e., H_n^+, where n is typically 2 or 3), or a metal-hydride-ion ($M_xH_y^{n+}$), for example TiH_2^+. There is a reported dependence on the crystallographic facets imaged by FIM (Martinka, 1981), where H can enhance the FIM contrast and resolution possibly through a modification of the electrostatic field distribution (Müller et al., 1965) and can facilitate field evaporation at relatively lower electrostatic fields (Rendulic & Knor, 1967). These complex mechanisms and fundamental questions remain to be fully clarified. Studies of field evaporation in FIM were mostly performed under constant electrostatic field conditions, whereas field evaporation in APT is triggered by high-voltage (HV) or laser pulses. Because of the time it takes for the H to migrate along the shank up to the imaged surface at the tip of the needle, the detected amount of hydrogen depends strongly on the time between field evaporation events, which is controlled through a combination of laser pulsing frequency and detection rate (Sundell et al., 2013; Kolli, 2017; Meier et al., 2023).

H and Field Evaporation

The presence of H can facilitate field evaporation of surface atoms at a relatively lower electrostatic field than in its absence (Müller et al., 1965; Wada et al., 1983). The evaporated ions can be in the form of hydrogen-bearing metal-hydride-ion ($M_xH_y^{n+}$), as noted by Krishnaswamy & Müller (1977). Different metallic elements show different propensities to form these hydride ions (Stepien & Tsong, 1998), and these should not be confused with hydrides as a phase present in the original sample in the thermodynamic sense. Zr and Ti are prone to forming evaporated hydrides in the 2+ charge state, which agrees with more recent reports (Mouton et al., 2018; Chang et al., 2019*b*) and was also discussed in the workshop (A. Diagne, CNRS-GPM, Rouen, France). Other hydrogenated ionic species have also been reported (Heck et al., 2014; Greer et al., 2020).

Another complexity related to H atom field evaporation is that H can be detected in various forms as mentioned previously, i.e., monatomic H^+, molecular H_2^+ and H_3^+, and as metal-hydride-ion (e.g., TiH^+, TiH_2^+). The distribution of their relative abundances depends on the strength of the electrostatic field (Tsong et al., 1983). The strength of the surface field is complex at the atomic scale, and may need to be assessed for each dataset individually and even for each of the analyzed microstructural feature of interest within a single APT dataset.

There are still many open questions. For instance, how does hydrogen behave with individual substitutional or interstitial elements constituting an alloy of interest? How it is supplied across the field-of-view? Why is H detected more at crystallographic poles or some particular crystallographic facets? Is H also subject to surface diffusion when originating from within the material? (Martinka, 1981; Gemma et al., 2011). If so, does it migrate towards protruding particles or precipitates that require a higher electrostatic field to field evaporate (Miller & Hetherington, 1991; Vurpillot et al., 2000)? If so, this could artificially increase its concentration near features such as carbides in steels (Breen et al., 2020) or precipitates in Zr alloys (Jenkins et al., 2023). Addressing these questions will require targeted studies, likely combining experiments along with theory and simulations.

Hydrogen and Deuterium

Finally, there are other challenges arising from the high mobility of H in most materials, which can enable H diffusion between specimen preparation, H-loading, specimen transfer, and even during the APT analysis itself. It should be noted that, herein, we use diffusion to refer generally to the motion of hydrogen through the material; this can be through traditional thermally activated diffusion processes or through athermal tunneling.

To some extent, this diffusion can be mitigated by using lower temperatures. Another option is the use of a coating on the surface that can act as a permeation barrier and help prevent out diffusion of H from the loaded sample (Hollenberg et al., 1995; Kremer et al., 2021). Nevertheless, H can also move or migrate by atomic tunneling through the lattice, which will limit the efficacy of using low temperatures—see Gemma et al. (2009) and references therein.

Deuteration, i.e., the use of deuterium (D or ^2H) in lieu of H, offers multiple advantages to facilitate quantitative analysis of H in materials by APT. Deuterium is a heavier isotope of H, with a natural abundance of only 0.0145 at%. Due to its slightly higher mass, it diffuses more slowly than H and its tunneling rate is lower (Maxelon et al., 2001). D is hence less prone to moving between specimen preparation and analysis, as well as during the analysis (Gemma et al., 2009). Even at low temperature, i.e., near 25K, diffusion of both H and D can occur. The composition profile for H and D across an Al_3Zr dispersoid reported by Zhao et al. (2022) shows a tendency for a higher concentration of H and D nearer to the freshly exposed surface during the analysis. Although this may be due to a locally higher misfit strain, the profile could be interpreted as a proof of diffusion during the experiment, as raised by Prof. A. Pundt (KIT) during the discussions.

Deuteration of the specimen itself can also alleviate some of the issues arising from the overlap with residual gaseous hydrogen as well. D should be detected at 2 Da and not 1 Da (Gemma et al., 2007, 2011; Takahashi et al., 2010; Haley et al., 2014); this is provided that the experimental conditions, particularly the intensity of the electrostatic field, are selected to minimize the detection of residual H in the form of H_2^+. Otherwise, the overlap between the two signals will not allow for distinguishing between the two ions as modern APs have insufficient mass resolution. As presented by Dr. K. Moore (University of Manchester) during the workshop (Li et al., 2019), NanoSIMS has sufficient mass resolution to distinguish between the two. The possibility of designing a novel atom probe with sufficient mass resolution was not discussed, but could be an interesting avenue of research in the future.

In some datasets, peak splitting has been observed for the 2 Da peak, which could enable differentiation between D^+ and H^{2+} ions (Meier et al., 2022). For a D-loaded W sample analyzed using laser assisted evaporation in a straight flight path instrument, a sharp peak is observed at the leading

Downloaded from https://academic.oup.com/mam/advance-article/doi/10.1093/mam/ozae081/7748435 by guest on 10 October 2024

edge of the 2 Da peak, which is not present in the unloaded sample. A broad peak at the trailing edge of the 2 Da peak is present in both the charged and uncharged sample. The number of ions contributing to the broad peak varies as a function of electrostatic field, whereas that of the sharp peak does not. This suggests the broad peak corresponds to the contaminant hydrogen species H_2^+, whereas the sharp peak could correspond to intentionally loaded D^+. Peak splitting is not observed when the same D-loaded sample is analyzed using a reflectron-fitted atom probe. This suggests that the contaminant species H_2^+ exhibits an energy deficit causing a difference in the time-of-flight that gets corrected by the time-of-flight-compensating reflectron optic.

Additionally, the complex field evaporation behavior of H-containing materials may also lead to complexities in the elemental or ionic identification of the peaks in the mass spectrum due to the overlap of hydride- and deuteride ions at the same mass-to-charge-state ratio (e.g., ZrH_2^+ and ZrD^+) (Mouton et al., 2018; Jones et al., 2022). This is particularly problematic in cases where a substantial fraction of the signal at 2 Da can be attributed to H_2^+.

It also often appears that following D-loading, a peak at 3 Da appears, despite the electrostatic field conditions selected such that H should be detected primarily as H^+ at 1 Da. This could be associated with an HD^+ ion from incomplete deuteration, i.e., the solution or gas used for H-loading contained a fraction of H, or to exchange between H and D during storage for instance. These exact mechanisms along with those responsible for other phenomena observed during APT analysis of H remain largely unexplained and will require further studies.

Optimizing H Analysis by APT

Figure 2 summarizes some of the key aspects discussed herein and during the workshop. These are all pieces of a larger,

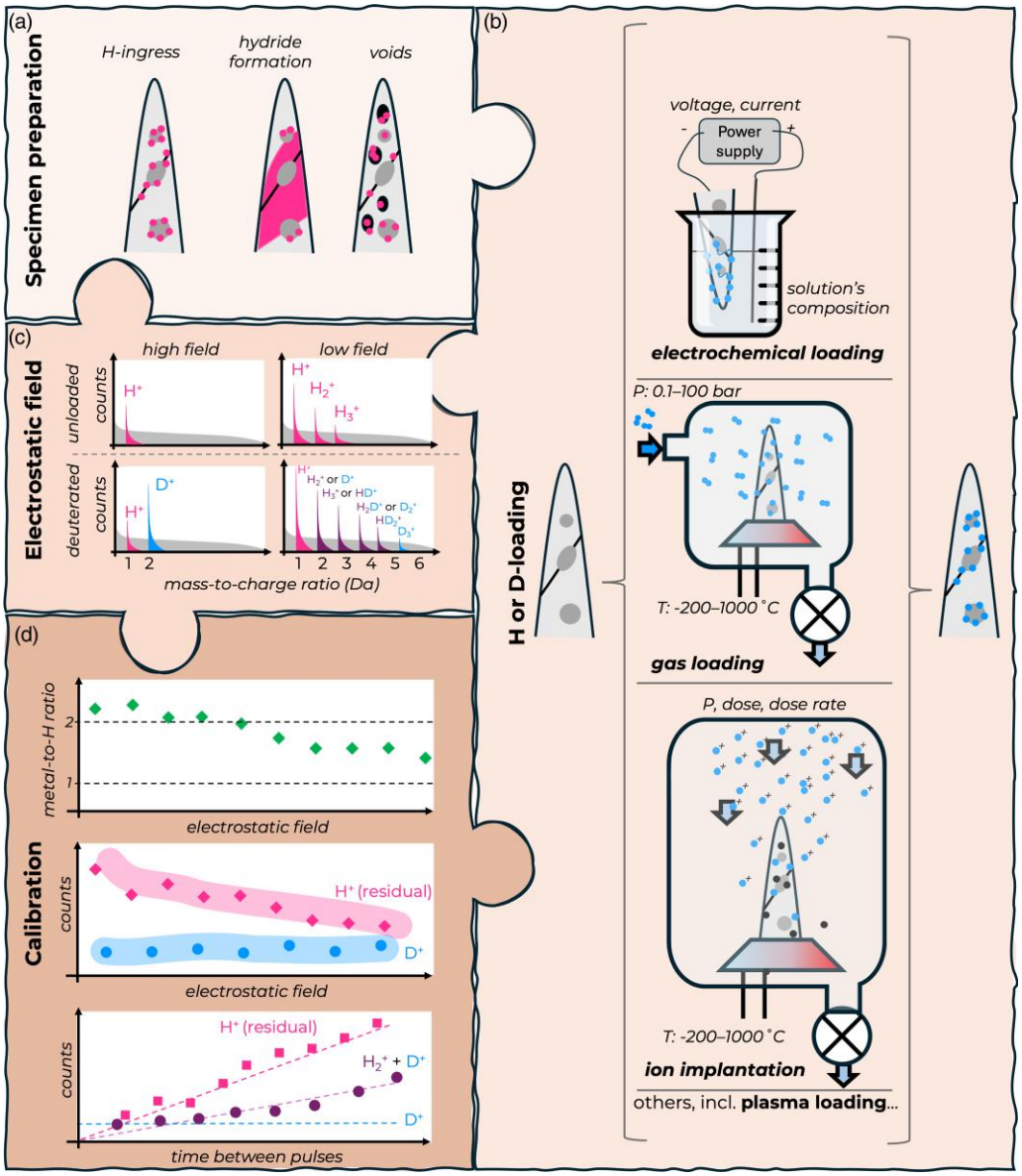

Fig. 2. Summary of the complexity of the analysis of H by APT: (**a**) ingress of H and structural damage from specimen preparation; (**b**) numerous methods for H- or D-loading and their most relevant parameters; (**c**) complexity of mass spectra obtained in different conditions of the electrostatic field; (**d**) possible calibrations needed to facilitate interpretation of H/D-analysis by APT.

Downloaded from https://academic.oup.com/mam/advance-article/doi/10.1093/mam/ozae081/7748435 by guest on 10 October 2024

complex puzzle. The following sections discuss specimen preparation (A), H-/D-loading methods (B), optimization of the electrostatic field conditions during analysis (C), and possible means and interests of performing calibrations (D).

Specimen Preparation

General Considerations

Specimens for APT must be prepared in the shape of sharp needles, with an end radius below approximately 100 nm. They can be prepared by electrochemical polishing from a blank, i.e., a small parallelopiped bar or a piece of wire of the material, typically 400 μm across and 1–3 cm long. An alternative route is to use a focused-ion beam (FIB) microscope, often coupled with a scanning electron microscope (SEM) (Prosa & Larson, 2017), or sometimes a combination of both (Miller & Russell, 2006). It should be noted that the process of specimen preparation may lead to some degree of stress relaxation, which can itself lead to rearrangement of dislocations within the sample potentially to hydrogen relocation.

Additionally, there are approaches to fabricate materials for analysis directly onto preshaped specimens after they have been cleaned by field evaporation. Many of the early studies of multilayers by APT were performed on thin films or multilayers deposited directly onto needle-shaped substrates (Larson et al., 2009). This was also the case for H-studies by Gemma et al. (Kesten et al., 2002; Gemma et al., 2007, 2011, 2012). These are not the most commonly analyzed samples.

H-ingress During Preparation

An additional complexity for studying H by APT was highlighted in the recent reports that point to the ingress of hydrogen during specimen preparation (Chang et al., 2018; 2019*a*; Yan et al., 2019; Breen et al., 2020; Mouton et al., 2021). In the case of Ti or Zr alloys, this had been reported in the preparation of specimens for electron microscopy (Banerjee & Williams, 1983; Ding & Jones, 2011; Hanlon et al., 2019), and may have been known to the APT community previously but only rarely reported (Parvizi et al., 2014). A comment in this direction was made at the APT&M 2018 conference in Gaithersburg, MD by Prof. G. Schmitz (University of Stuttgart).

Following preparation of a specimen from a pearlitic steel by electrochemical polishing, Breen et al. (2020) reported substantial amounts of H. The amplitude of the H signal dropped substantially following heating at moderate temperature (<150°C). They interpreted this as a proof that H had been introduced into the specimen during the sharpening process because of uncontrolled electrochemical conditions that formed atomic hydrogen on the surface and lead to unintended uptake and H-loading. This H can diffuse into the material and saturate the microstructural traps, thereby preventing efficient D-loading into the traps. In previous discussions at APT&M conferences, the group at the University of Oxford revealed unpublished results that contradict this position. They said that the preparation of APT specimens using fully deuterated solutions throughout the electrochemical polishing process did not result in a similar deuteration of the specimen (Chen, 2017). This point will hence require additional systematic experiments to be further clarified.

Evidence has pointed to the introduction of significant amounts of H in Ti and Ti-alloys, and in Zr alloys during the final stages of specimen shaping during FIB-based specimen preparation at room temperature. In this case, it is assumed that the H originates from the corrosion of the freshly created surface by the residual moisture inside the FIB which, through water splitting, leads to atomic H on the specimen surface. It is also possible that other gaseous species present inside the vacuum chamber of the SEM-FIB including hydrocarbon or simply H_2 are dissociated on the surface, thereby forming atomic H. Once created, atomic H can penetrate inside the sample particularly through phases that have a high solubility for H, e.g., β-Ti (Chang et al., 2018; Yan et al., 2019) or through microstructural defects, e.g., grain boundaries (Chang et al., 2018). The H can accumulate to such an extent where a hydride phase (i.e., TiH or ZrH_2) forms at room temperature. No such reports exist for steel and ferrous-alloys, but corrosion could also lead to H formation and ingress (Eliezer et al., 1979; Holroyd, 1988; Parvizi et al., 2017) in those materials. Cryogenic specimen preparation by FIB has been reported to prevent (or at least drastically limit) the pick-up of H during FIB-preparation of Ti- and Zr- based alloys (Chang et al., 2019*a*; Mouton et al., 2021; Jenkins et al., 2023; Mayweg et al., 2023). This may be related to a combination of moisture being trapped by the cold finger or the cryostage, as well as with a reduction of the kinetics of water splitting or of the diffusivity of hydrogen.

Ion and Electron-Beam Damage

Beyond the formation of hydrides, FIB-based preparation was shown to induce potential structural damage in the form of vacancies (Larson et al., 1999; Miller & Russell, 2006). Considering the high trapping energy of hydrogen by vacancies in most metallic systems (Canto et al., 2014), introducing vacancies during preparation could affect the existing hydrogen distribution. Recently, Saksena et al. (2023) reported void formation from the agglomeration of FIB-induced vacancies that affected the H–H– capabilities of two-phase steels, as a high fraction of the loaded D was trapped in these voids. They offered a possible specimen preparation workflow that minimizes these issues by using electron-beam Pt deposition for protection, and then using a Xe-plasma FIB during sharpening.

A final aspect that was discussed following the presentation of Dr. D. Mayweg (Chalmers University) is the possible need to prepare specimens along specific crystallographic orientations, since the distribution of H or D, along with H- or D-containing molecular ions, is dependent on the crystallographic facets in the specimen apex region (Martinka, 1981; Chang et al., 2019*b*). This is particularly important in cases where calibrations are performed so that similar orientations are compared. This may require imaging the surface before H-loading by electron-backscattered diffraction, or the use of transmission Kikuchi diffraction (Babinsky et al., 2014) or TEM (Henjered & Norden, 1983) sequentially during the preparation to ensure that a grain with the appropriate orientation is located at the tip of the specimen. This approach may come with the caveat that structural damage can be induced by the recoil of surface species under electron-beam illumination (Gault et al., 2023). Cold traps inside the microscope or intermediate specimen cleaning by low-energy Ar milling (Herbig & Kumar, 2021) could help reduce the contamination. Structural defects generated from this recoil-associated damage can affect the subsequent distribution of H or D after loading.

Downloaded from https://academic.oup.com/mam/advance-article/doi/10.1093/mam/ozae081/7748435 by guest on 10 October 2024

Specimen Transport and Vacuum-Cryo-transfers

Corrosion leading to the creation and ingress of atomic hydrogen at the surface could also occur during exposure to atmosphere during preparation or transfer of specimens into the atom probe chamber. Transfer is conventionally performed in ambient atmosphere, but can be mitigated by the use of vacuum shuttles, sometimes referred to suitcases. Vacuum shuttles also offer the possibility to perform the transfer at cryogenic temperature, which is achieved by using liquid nitrogen. Such a workflow offers the advantage of limiting the thermally activated diffusion of trapped H and mobile or trapped D throughout the microstructure. This combination of high- or ultrahigh-vacuum levels prevent frost formation, and cryogenic suitcases are increasingly available in APT facilities across the world (Chen et al., 2017*b*, 2019; Stephenson et al., 2018; McCarroll et al., 2020).

To limit the exchange with the atmosphere during transport, an alternative could be to follow H-loading with protection of the surface by using a conformal coating of a material with very limited permeability for H or D. For instance, H or D inside an uncoated specimen can reach the surface, recombine, and desorb. This can deplete the subsurface region and create a gradient that can drive further diffusion of H or D from the inner part of the specimen towards the surface. A coating could slow down this outgassing, the associated diffusional processes, and prevent such a gradient. Conformal coatings of APT specimens have been reported (Seol et al., 2016; Adineh et al., 2018; Kim et al., 2022). Recently, the means to conformally coat APT specimens directly *in situ* in the FIB have been reported (Schwarz et al., 2024), including at cryogenic temperature (Zhang et al., 2021; Woods et al., 2023). However, these coatings are typically metallic in nature and may not offer the necessary impermeability for H or D. Forming an oxide coating by using e.g., an oxygen-based plasma or dosing O into the chamber could be a way to form a conformal coating with a lower H permeability (Kremer et al., 2021).

Full cryogenic workflows including (site-specific) specimen preparation by FIB lift-out (Schreiber et al., 2018; Douglas et al., 2023), surface protection, transport into the atom probe to analysis can be performed. However, the use of such workflows has not yet been reported to study the distribution of H or D.

Loading with H or D

Loading Modes

Loading with H and D has been accomplished through electrochemistry (Haley et al., 2014), gas-phase (Gemma et al., 2012; Khanchandani et al., 2022*a*), or ion implantation (Walck & Hren, 1984; Daly et al., 2021*b*) methods. The use of a H-rich plasma has also been mentioned (Maier et al., 2019). Note that workflows have been introduced for loading with H, D, and also tritium (T), and it is important to keep in mind that they will all behave slightly differently through small differences in adsorption energy and mobility through the material due to their slightly differing mass.

The optimal conditions for loading will depend on numerous parameters. Electrolytic or cathodic H-loading is performed in a solution. The key parameters are the voltage, current, the solution composition including the acid concentration, and the presence of an inhibiter that hinders the recombination of atomic H into H_2, and the temperature at which the loading is performed. Other subtle or unexpected parameters could also be critical—for instance, using Pt as a counter electrode can lead its dissolution and deposition of Pt on the cathode (Chen et al., 2017*a*). Also, the pH of the solution may need careful monitoring as it can be modified by dissolved species from the atmosphere and might require purging by N_2 or Ar (Anantharaj & Noda, 2022).

For gaseous H-loading, the temperature, the nature of the gas, and, importantly, its purity (Fromm & Uchida, 1987) and pressure all matter. Numerous designs of cells enabling gas thermochemical treatments of atom probe specimens have been proposed (Bagot et al., 2006; Dumpala et al., 2014; Haley et al., 2017; Perea et al., 2017; Khanchandani, et al., 2022*a*). High temperatures can be achieved through resistive heating or recently by using a DC laser. The laser offers the advantage of temperature control that can be difficult to achieve through resistive heating including complex heat treatment schedules and very fast cooling. Cryo-cooling may assist in capturing sensitive transient states (El-Zoka et al., 2023) but can result in the subsequent condensation of contamination on the specimen that can preclude further analysis (e.g., via TEM) without additional cleaning (Herbig & Kumar, 2021). Ultimately, precise calibration of the temperature through thermocouples is typically necessary, particularly as pyrometers often neglect to account for nonideal emissivity of the targeted sample that has a surface state that can have changed during exposure to the gas.

Finally, with regards to ion implantation, the dose and dose rates are important, but so is the surface state. It has been reported that C-based species can be carried into the material during ion implantation (Dagan et al., 2015) due to the overall cleanliness of the vacuum inside the implanter (Wang et al., 2017).

Loading Efficacy

There is an overarching need to measure the efficacy of the H-loading process to optimize the loading conditions. For instance, Takahashi et al. (2010, 2012) noted that H-loading at a higher temperature can favor uptake. Depending on the material, H permeation through a surface oxide layers can be very difficult, slow, or near impossible (Evers et al., 2013), and will likely depend on the temperature. The formation of atomic H may need to be assisted or catalyzed by other metals. Dr. M. Rohwerder (MPISUSMAT) mentioned the use of a thin film of Pd deposited onto the sample of interest when doing Kelvin probe experiments for instance (Kesten et al., 2002; Lupu et al., 2004; Gemma et al., 2009). Coatings deposited using the approach of Schwarz et al. (2024) can be made to cover the entire specimen or only a part of the surface. This opens an opportunity for depositing Pd on a section of the specimen to favor the formation of atomic H on the surface and possibly facilitate H- or D-loading. Cathodic H-loading has most often been reported on specimens prepared from electrochemical polishing; a site-specific specimen prepared by FIB lift-out presents additional challenges. The weld used for mounting the FIB lift-out is typically made of a Pt-C or W-C composite, with a density that depends on the exact deposition conditions and whether an electron or ion beam is used (Felfer et al., 2012). The volume of material to be analyzed is slow, and with a high surface-to-volume ratio. Both the weld and the material of interest can corrode quickly or be completely lost (Khanchandani et al., 2022*b*). The thickness of the welds

Downloaded from https://academic.oup.com/mam/advance-article/doi/10.1093/mam/ozae081/7748435 by guest on 10 October 2024

must be adjusted to accommodate this loss. To increase the success rate, the sample should be loaded before the final sharpening is performed (Khanchandani et al., 2022*b*), preferably at low temperature as discussed above. The possibility of using redeposition welding followed by a metallic reinforcement should be explored in the future (Douglas et al., 2023; Woods et al., 2023).

The high diffusivity of H, and to a lesser extent D, can lead to a loss by outward diffusion and possible recombination and desorption on the surface (Fig. 1b) that is facilitated by the necessarily small size of the needle-shaped APT specimens (Gemma et al., 2009; Haley et al., 2014). This makes the transfer time, temperature, and pressure critical parameters that need to be reported to facilitate reproducibility of results. For instance, exposure of samples to ambient atmosphere can lead to possible oxidation or corrosion reactions (with moisture) on the freshly prepared specimen surface. This can lead to the release of atomic hydrogen from the splitting of water that can then penetrate into the material (Rodrigues & Kirchheim, 1983; Gråsjö et al., 1995). The opposite process could also take place. The formation of water on the surface that could favor a depletion of H from within the specimen. This water could subsequently evaporate under ambient conditions. Such a reaction could lead to exchange between H and D in the near surface region with H from residual moisture, thus lowering the relative amplitude of the D signal. At low temperatures the formation of ice on the specimen surface could act as a barrier, or it may simply limit the kinetics of these reactions.

Cryogenic Cooling

Cryogenically cooling specimens immediately after H-loading can slow the outward diffusion of H or D (Takahashi et al., 2010; Chen et al., 2017*b*; Takahashi et al., 2018) and facilitate detection. This requires substantial dedicated infrastructure (Perea et al., 2017; Stephenson et al., 2018). Using vacuum and cryo-transfer can avoid frosting of cold specimens transported through ambient atmosphere and protect the reactive surfaces of freshly prepared specimens from the environment. However, a lower H pressure in the surrounding atmosphere might facilitate outgassing. In addition, as noted above, there is a regime of athermal H-migration by tunneling that cannot be avoided even by the use of cryogenic transfer. Another consideration is that at a lower temperature, the solubility of H or D into a given phase will likely decrease (Fig. 1c), making it possible for hydrides to form or simply artificially changing the partitioning between different phases compared to what it would be at higher operating temperatures for materials in service conditions.

Finally, it should be noted that since H and D are typically fast diffusers in body-centered cubic α-Fe, if diffusible hydrogen is to be analyzed then fast cooling following H-loading should be envisaged. This has so far been achieved primarily using liquid nitrogen, but there may be ways to use other coolants as for cryo-TEM (Dubochet, 2016). Chen et al. (2017*b*, 2019) reported losses in the case of the analysis of some carbides.

However, this is not *always* necessary even in ferritic or martensitic steels. H- or D- can be strongly trapped at microstructural features where higher temperatures are required to induce de-trapping at a sufficiently high rate. This information is typically accessible via TDS for instance. Please note, even in TDS, the detected amount of H is dependent on the size of specimens (Suzuki & Takai, 2012). Ultimately, there have been several reports of analysis of hydrogenated, deuterated, or tritiated samples with no cryogenic holding, preparation, or transfer leading to successful detection of D/T at certain microstructural features (Devaraj et al., 2021; Sun et al., 2021; Wang et al., 2022; Khanchandani et al., 2023; Jakob et al., 2024).

Experimental Analysis Conditions

An important aspect introduced in Section 2.2 is that residual H can be detected in the form of H^+, H_2^+, and H_3^+ (Krishnaswamy & Müller, 1977; Tsong et al., 1983; Wada et al., 1983), with a distribution that exhibits a strong dependence on the surface electrostatic field conditions (Fig. 1b). How these various ionic species form and then dissociate under the effect of the intense electrostatic field (Tsong et al., 1983; Ai & Tsong, 1984) remains an open question, in part because of the complex physics involved (Xu et al., 2017). Clarification of this issue will require targeted studies.

To a first approximation, and according to the postionization theory (Kingham, 1982), the charge-state ratio can be used to monitor the electrostatic field conditions across datasets and instruments (Shariq et al., 2009). It should be noted that the actual absolute values of the field derived from the theory may be inaccurate; examples have been reported where the theory does not readily apply in semiconductors or oxides (Schreiber et al., 2014; Cuduvally et al., 2022; Singh et al., 2024) due to a more complex field evaporation behavior or field-induced dissociations. The charge state of atomic ions can often be used (Kellogg, 1982), but the relative abundance of molecular ions also shows similar trends (Müller et al., 2011), even if their precise formation mechanisms can remain elusive. The ratio of a combination of atomic and molecular ions was used in the case of the analysis of bulk hydrides (Chang et al., 2019*b*).

In deuterated samples, the consensus appears to be that when HV pulsing is possible, then it should be used. HV pulsing leads to higher electrostatic fields and hence reduces the relative fraction of H_2^+ and H_3^+, making it easier to discriminate D-containing peaks. That said, there are issues with operating at higher fields. For example, at higher fields the relative fraction of multiple events increases, which can lead to more severe ion pile up at the detector and losses of H or D, as discussed in Chang et al. (2019*b*). Laser pulsing facilitates field evaporation at relatively lower electrostatic fields, which promotes the detection of relatively higher levels of residual H and of multiple H-containing species, including possible combinations of D and H that can make peak identification highly complex; Figure 2c (Mouton et al., 2018; Jones et al., 2022). A relatively lower electrostatic field tends to improve yield (Prosa et al., 2019), and in some cases using laser pulsing may be the only way to get any data at all.

It is often the case that experiments are run at a constant detection rate, i.e., a fixed average number of ions detected per pulse. However, as the specimen blunts as it is eroded during the experiment, the emitting area gradually increases, and maintaining the detection rate forces a monotonous slow overall decrease in the electrostatic field in HV pulsing mode. In laser pulsing mode, the situation can be made more complex as a relatively larger specimen volume results in a lower peak temperature for the thermal pulse, which is compensated by a

Downloaded from https://academic.oup.com/mam/advance-article/doi/10.1093/mam/ozae081/7748435 by guest on 10 October 2024

relative increase in the electrostatic field. There is an important optimization process to pursue here, and careful calibrations are the only way to assess if the amount of detected H or D is statistically significant.

Calibrations

For decades, APT has been claimed to be calibration-free since the technique relies on counting the number of individual ions of each species. This is expected to contrast with electron-probe microanalysis, energy-dispersive X-ray spectroscopy or SIMS for example, for which standards of known compositions are normally necessary for regular calibration and accurate quantification. However, this claim is known to be wrong—a report in the 1980s already showed species-specific losses from the field evaporation at the DC voltage of the element with the relatively lower evaporation field (Miller & Smith, 1981). In the time-of-flight spectrum, ions formed from DC-field evaporation, lost from the analysis, combine with the dark current of the detector to form a level of white background. Upon conversion into mass-to-charge ratios, this can result in a dependency of the measured background and composition on the base temperature and pulsing frequency (Hyde et al., 2011; El-Zoka et al., 2020; Hatzoglou et al., 2020; Cappelli & Pérez-Huerta, 2023).

There are other loss mechanisms that can affect the quantifiability of the measurements. First, two or more ions of similar mass-to-charge emitted by a single pulse and flying along similar trajectories can hit the detector in too close spatial or time proximity for both to be detected (Rolander & Andrén, 1989). This so-called pile-up effect was studied in detail for B (Meisenkothen et al., 2015) and C (Peng et al., 2018) on modern commercial instruments. Second, dissociation of molecular or cluster ions during the flight can produce neutral atoms or molecules (Gault et al., 2016) that have a strong dependence on the electrostatic field conditions (Zanuttini et al., 2017). Tracks in the correlation histogram for multiple events (Saxey, 2011) normally reveal these dissociation reactions in straight flight path instruments, and allow for identifying the corresponding reactions, e.g., $MO_2^+ \rightarrow M^+ + O_2$. To a first approximation, the relative energetic stability of the end products ($M^+ + O_2$), with respect to the parent molecular or cluster ion (MO_2^+), provides a guide for estimating if a dissociation can lead to the formation of a neutral atom or molecule (Blum et al., 2016; Gault et al., 2016; Zanuttini et al., 2017, 2018; Kim et al., 2024). Through one or more of these loss mechanisms, compositional inaccuracies have been reported for oxides, carbides, and nitrides as well as for metals (Sha et al., 1992; Marquis, 2007; Müller et al., 2011; Thuvander et al., 2011; Amouyal & Seidman, 2012; Marceau et al., 2013; Mancini et al., 2014). All exhibit a dependence on the electrostatic field conditions. Ultimately, the question remains if and how these effects impact the analysis of hydrogen by APT.

For analysis of H by APT, one could envisage the analysis of an "H standard". This is common practice across fields and for other techniques, including X-ray energy or wavelength dispersive spectroscopy and SIMS. Some material standards were also used to compare with APT across other analysis techniques (Meisenkothen et al., 2015; Exertier et al., 2018; DeRocher et al., 2022).

During the discussions, it was proposed to use stable hydrides that can be sourced commercially, such as TiH_2. Chang et al. (2019*b*) analyzed a series of specimens prepared from a freshly fractured surface of a stable TiD_2 sample. They reported the formation of D_2 through the reaction $TiD_2^+ \rightarrow Ti^+ + D_2$ along with multiple events containing two D^+ ions that could lead to substantial pile-up. There is also delayed field evaporation that will lead to losses to the background. These mechanisms are all dependent on the amplitude of the electrostatic field, which was monitored by the ratio between charge states Ti^{3+} and Ti^{2+} or Ti^{2+} and TiD_2^+.

There is another perspective on the necessity for calibration, which is that the amount of residual H and the corresponding ionic distribution (i.e., the relative amplitudes of H_n^+, where $1 \leq n \leq 3$) can be expected to be reproducible from one experiment to another on a similar instrument, or set of instruments. This was reported for a range of metallic materials as a function of the charge-state ratio of one of the elements within the material (Breen et al., 2020; Kim, et al., 2022; López Freixes et al., 2022; Khanchandani et al., 2023; Meier et al., 2023) and can offer a way to assess whether the measured content of H (or D) falls within the possible range of detectable H in unloaded specimens, or whether the difference is statistically significant. This was also performed on a local basis within the microstructure, since the charge-state ratio is locally accessible (Chang et al., 2018).

Finally, Meier et al. (2022) introduced an alternative calibration by investigating the variations in the detected amount of H^+ and H_2^+/D^+ as a function of the time between two pulses. This is based on the assumption that H-migrates along the specimen shank, and hence the supply of H to the emitting area at the tip of the specimen will be time dependent. A series of experiments were done at varying pulse frequencies and detection rates, with the caveat that the electrostatic field changed in the latter case. With a shorter time between pulses, the supply of H and hence the detection of H^+ and H_2^+ should be limited, but the detection of D should not. This approach was used across several materials and data reported and discussed on multiple occasions.

Although such approaches do not provide an actual calibration in the metrology sense, they help provide trends as to the levels of H that can be expected under a certain range of electrostatic field conditions. This offers a comparison point as to how far off this trend a particular measurement can be, supporting interpretation of the statistical significance of a locally measured high H- or D-concentration (Breen et al., 2020; López Freixes et al., 2022; Khanchandani et al., 2022*b*).

Recommendation for APT Data Reporting

Focusing on the analysis of geological materials, Blum et al. (2018) proposed a set of parameters that should be recorded and reported for each APT dataset used in scientific publications. The table they proposed contains critical information to facilitate the analysis of the data by an external expert reader. Similar information had been previously proposed by Diercks et al. in an extended abstract (Diercks et al., 2017), as mentioned by Dr. S. Gerstl (SCOPEM, ETH Zurich) during the workshop.

We propose to use a modified and extended version of the table from Blum et al. that can be downloaded as a spreadsheet from this link:

https://docs.google.com/spreadsheets/d/1nt5n6uBHsCnv_30RWw–U9lo2vDZW1iWF50LGd2rd7s/edit?usp=sharing

A copy is also available in the Supplementary Information. In putting together this spreadsheet, we tried to align with

Downloaded from https://academic.oup.com/mam/advance-article/doi/10.1093/mam/ozae081/7748435 by guest on 10 October 2024

current efforts in defining an APT-focused ontology to capture relevant metadata to facilitate storage and reuse of data according to the FAIR principles (Wilkinson et al., 2016). The FAIRMAT project, a part of the German's national research data management initiative, appears today to contain the most complete listing available for APT; see link in the Supplementary Information.

We also generally agreed that it would be best to always attempt to include a set of additional information in the Supplementary Information of manuscripts. First, a mass spectrum, with absolute and not relative counts—i.e., not just a normalized spectrum. This will help assess the statistical significance of peaks overall. Ideally, the mass spectrum should be visually readable, so maybe splitting it into various parts may help. Ideally, the spectrum should be supplied also as a.csv file supplemented by the range file. Second, whenever possible, electron micrographs of specimens should also be included. Ideally, images should be provided at a range of magnifications to assess the shape further down the shank. Third, in the case of H-loading through ion implantation, simulated profiles from calculations of the stopping range of ions in matter (Ziegler & Biersack, 1985) should be included.

We believe that these recommendations could and should be followed more generally across the field, but we propose that all workshop attendees use this from now on to report H data in their own scientific articles and suggest their adoption during peer-review of scientific articles focused on the topic.

Perspectives and Conclusion

In summary, H analysis by APT is still far from routine. The experimental methods and analysis depend on the exact materials science question that is to be addressed. There are many effects that compound to make the analysis extremely complex, with numerous parameters that must be accounted for and appropriately reported to ensure reproducibility of the experiments. Figures 1 and 2 summarize some of the key aspects discussed herein and during the workshop.

Depending on whether one aims to measure H in low concentration in solid solution, or a higher amount of H segregated at microstructural features, or finally the composition of hydrides, the analyst will face very different challenges. The first requires low H background, and adjusting the electrostatic field conditions to avoid the detection of H_2^+ so D^+ can be confidently labeled and measured. The second also requires a low background level, but must include careful analysis of the local field conditions that can change drastically at individual microstructural features. The third appears less problematic, i.e., at least it faces familiar problems with APT in general in terms of the estimation of stoichiometry of known compounds, with a strong dependence on the electrostatic field conditions. Calibration with analyses carried out on reference samples might be required, especially for the first and third cases, but also a calibration of the expected H contents and distributions as a range of electrostatic field conditions can inform on the statistical significance of local high H or D concentrations. Such a calibration can be made on an unloaded specimens aiming at determining the conditions (i.e., a specific charge-state ratio) that minimizes the influence of residual hydrogen on the analysis.

The good news is that it seems that the community is, on average, more careful in drawing conclusions from observations of H by APT than it has sometimes been with other elements that are notoriously difficult to quantify. This is a good thing. Reports have historically been limited to qualitative statements, since quantification is extremely challenging. The development of novel instruments with lower levels of residual hydrogen may hold the key for more accurate measurements in the future. We will not be able to perform quantitative analysis without understanding the details of the origins of the signal. More fundamental understanding of the behavior of H near the surface of the field emitter is therefore needed to go beyond "the hero experiment" and really reach routine, reproducible, and defensible quantitative analyses.

Finally, the question of required accuracy needs to be addressed. For example, what is the required accuracy of an H concentration measurement that is needed to properly inform modeling and then answer materials science questions? Given a measured concentration, what accuracy is required to distinguish between models of plasticity-mediated embrittlement and decohesion mechanisms? When planning such highly demanding APT experiments, it is also important to consider the difference between ideal, laboratory H- or D-loaded measurements performed under carefully controlled scenarios versus the actual service conditions that engineering parts would see. There are likely to be great differences in atmosphere, temperature, pressure, exposure time, and possibly stress. Nevertheless, APT remains a powerful technique for three-dimensional H mapping, localized H quantification, and indeed for understanding the behavior of H in complex microstructures. Its impact will only continue to grow with our understanding of the origins of H in APT experiments and the behavior of H under high field conditions.

Availability of Data and Materials

The authors have declared that no datasets apply for this piece.

Supplementary Material

To view supplementary material for this article, please visit https://doi.org/10.1093/mam/ozae081.

Acknowledgments

This workshop was organized and chaired by Aparna Saksena, Baptiste Gault, Xavier Sauvage, and Paul Bagot and sponsored by the International Field Emission Society (IFES, http://www.fieldemission.org/). The organizers are grateful for financial support by Thermofisher Scientific, Cameca Instrument, and Ferrovac. Apart from the corresponding authors, and the chairs, the authors were listed alphabetically. The editors Ann Chiaramonti & John Mansfield are thanked for proof reading and providing valuable feedback. Uwe Tezins, Andreas Sturm, and Christian Bross are thanked for technical support with the atom probe facility at the MPI SUSMAT. B.G. acknowledges financial support from the ERC-CoG-SHINE-771602. The APT group at MPI SUSMAT is grateful to the Max-Planck Gesellschaft and the BMBF for the funding of the Laplace Project, the BMBF for the UGSLIT project. B.G. and A.S. are grateful for funding from the DFG for SFB TR103/A4, and the CRC 1625/B4. T.M.S. is grateful for funding from the DFG through the award of the Leibniz Prize 2020. J.D. is grateful for support via EPSRC grant EP/V007661/1. R.G. thanks to Japan Society for the Promotion of Science (JSPS) KAKENHI via Grant Number JP24K08249. B.M.J. is a recipient of the WINNINGNormandy Program

Downloaded from https://academic.oup.com/mam/advance-article/doi/10.1093/mam/ozae081/7748435 by guest on 10 October 2024

supported by the Normandy Region and would like to acknowledge that this project has received funding from the European Union's Horizon 2020 research and innovation programme under the Marie Skłodowska-Curie grant agreement No. 101034329. M.K. acknowledges financial support from the DFG through DIP Project No. 450800666. P.F. and B.O. work has received funding from the European Research Council (ERC) under the European Union's Horizon 2020 Research and Innovation Programme (Grant Agreement No. 805065). L.D. acknowledges support from STFC grants ST/Y004817/1, ST/T002328/1, and ST/W001128/1.

Financial Support

The current study hasn't received any fund from any organizations or institutions.

Conflict of Interest

The authors declare that they have no competing interest.

References

Aboura Y & Moore KL (2021). NanoSIMS analysis of hydrogen and deuterium in metallic alloys: Artefacts and best practice. *Appl Surf Sci* **557**, 149736. https://doi.org/10.1016/j.apsusc.2021.149736

Adineh VR, Zheng C, Zhang Q, Marceau RKW, Liu B, Chen Y, Si KJ, Weyland M, Velkov T, Cheng W, Li J & Fu J (2018). Graphene-enhanced 3D chemical mapping of biological specimens at near-atomic resolution. *Adv Funct Mater* **28**, 1801439. https://doi.org/10.1002/adfm.201801439

Ai C & Tsong TT (1984). Field promoted and surface catalyzed formation of H3 and NH3 on transition metal surfaces: A pulsed-laser imaging atom-probe study. *Surf Sci* **138**, 339–360. https://doi.org/10.1016/0039-6028(84)90252-8

Amouyal Y & Seidman DN (2012). Atom-probe tomography of nickel-based superalloys with green or ultraviolet lasers: A comparative study. *Microsc Microanal* **18**, 971–981. https://doi.org/10.1017/S1431927612001183

Anantharaj S & Noda S (2022). Dos and don'ts in screening water splitting electrocatalysts. *Energy Adv* **1**, 511–523. https://doi.org/10.1039/D2YA00076H

Babinsky K, De Kloe R, Clemens H & Primig S (2014). A novel approach for site-specific atom probe specimen preparation by focused ion beam and transmission electron backscatter diffraction. *Ultramicroscopy* **144**, 9–18. https://doi.org/10.1016/j.ultramic.2014.04.003

Bagot PAJ, Visart de Bocarmé T, Cerezo A & Smith GDW (2006). 3D atom probe study of gas adsorption and reaction on alloy catalyst surfaces I: Instrumentation. *Surf Sci* **600**, 3028–3035. https://doi.org/10.1016/j.susc.2006.05.026

Banerjee D & Williams JC (1983). The effect of foil preparation technique on interface phase formation in Ti alloys. *Scripta Metallurgica* **17**, 1125–1128. https://doi.org/10.1016/0036-9748(83)90467-2

Bhadeshia HKDH (2016). Prevention of hydrogen embrittlement in steels. *ISIJ Int* **56**, 24–36. https://doi.org/10.2355/isijinternational.ISIJINT-2015-430

Blum I, Rigutti L, Vurpillot F, Vella A, Gaillard A & Deconihout B (2016). Dissociation dynamics of molecular ions in high DC electric field. *J Phys Chem A* **120**, 3654–3662. https://doi.org/10.1021/acs.jpca.6b01791

Blum TB, Darling JR, Kelly TF, Larson DJ, Moser DE, Perez-Huerta A, Prosa TJ, Reddy SM, Reinhard DA, Saxey DW, Ulfig RM & Valley JW (2018). Best practices for reporting atom probe analysis of geological materials. In *Microstructural Geochronology: Planetary Records Down to Atom Scale*, Moser DE, Corfu F, Darling JR, Reddy SM, Tait K (Eds.), pp. 369–373. Washington, DC: American Geophysical Union. https://doi.org/10.1002/9781119227250.ch18

Brandon DG (1963). Resolution of atomic structure—Recent advances in theory and development of field ion microscope. *Br J Appl Phys* **14**, 474–484. https://doi.org/10.1088/0508-3443/14/8/305

Breen AJ, Mouton I, Lu W, Wang S, Szczepaniak A, Kontis P, Stephenson LT, Chang Y, da Silva AK, Liebscher CH, Herbig M, Gault B, Kwiatkowski da Silva A, Liebscher CH, Raabe D, Britton TB, Herbig M & Gault B (2018). Atomic scale analysis of grain boundary deuteride growth front in Zircaloy-4. *Scr Mater* **156**, 42–46. https://doi.org/10.1016/j.scriptamat.2018.06.044

Breen AJ, Stephenson LT, Sun B, Li Y, Kasian O, Raabe D, Herbig M & Gault B (2020). Solute hydrogen and deuterium observed at the near atomic scale in high-strength steel. *Acta Mater* **188**, 108–120. https://doi.org/10.1016/j.actamat.2020.02.004

Canto G, Salazar-Ehuan I, González-Sánchez J, Tapia A, Quijano R & Simonetti S (2014). Density functional theory study of the hydrogen storage in a vacancy zone of an iron–nickel cell. *Int J Hydrogen Energy* **39**, 8744–8748. https://doi.org/10.1016/j.ijhydene.2013.12.039

Cappelli C & Pérez-Huerta A (2023). Testing the influence of laser pulse energy and rate in the atom probe tomography analysis of minerals. *Microsc Microanal* **29**, 1137–1152. https://doi.org/10.1093/micmic/ozad057

Cerezo A, Clifton PH, Galtrey MJ, Humphreys CJ, Kelly TF, Larson DJ, Lozano-Perez S, Marquis EA, Oliver RA, Sha G, Thompson K, Zandbergen M & Alvis RL (2007). Atom probe tomography today. *Mater Today* **10**, 36–42. https://doi.org/10.1016/S1369-7021(07)70306-1

Chang Y, Breen AJ, Tarzimoghadam Z, Kürnsteiner P, Gardner H, Ackerman A, Radecka A, Bagot PAJ, Lu W, Li T, Jägle EA, Herbig M, Stephenson LT, Moody MP, Rugg D, Dye D, Ponge D, Raabe D & Gault B (2018). Characterizing solute hydrogen and hydrides in pure and alloyed titanium at the atomic scale. *Acta Mater* **150**, 273–280. https://doi.org/10.1016/j.actamat.2018.02.064

Chang Y, Lu W, Guénolé J, Stephenson LT, Szczpaniak A, Kontis P, Ackerman A, Dear F, Mouton I, Zhong X, Zhang S, Dye D, Liebscher CH, Ponge D, Korte-Kerze S, Raabe D & Gault B (2019*a*). Ti and its alloys as examples of cryogenic focused ion beam milling of environmentally-sensitive materials. *Nat Commun* **10**, 942. https://doi.org/10.1038/s41467-019-08752-7

Chang YH, Mouton I, Stephenson L, Ashton M, Zhang GK, Szczpaniak A, Lu WJ, Ponge D, Raabe D & Gault B (2019*b*). Quantification of solute deuterium in titanium deuteride by atom probe tomography with both laser pulsing and high-voltage pulsing: Influence of the surface electric field. *New J Phys* **21**, 053025. https://doi.org/10.1088/1367-2630/ab1c3b

Chen R, Yang C, Cai W, Wang H-Y, Miao J, Zhang L, Chen S & Liu B (2017*a*). Use of platinum as the counter electrode to study the activity of nonprecious metal catalysts for the hydrogen evolution reaction. *ACS Energy Lett* **2**, 1070–1075. https://doi.org/10.1021/acsenergylett.7b00219

Chen Y (2017). *Characterisation of hydrogen trapping in steel by atom probe tomography*. PhD Thesis. University of Oxford.

Chen YS, Bagot PAJ, Moody MP & Haley D (2019). Observing hydrogen in steel using cryogenic atom probe tomography: A simplified approach. *Int J Hydrogen Energy* **44**, 32280–32291. https://doi.org/10.1016/j.ijhydene.2019.09.232

Chen Y-S, Haley D, Gerstl SSA, London AJ, Sweeney F, Wepf RA, Rainforth WM, Bagot PAJ & Moody MP (2017*b*). Direct observation of individual hydrogen atoms at trapping sites in a ferritic steel. *Science* **355**, 1196–1199. https://doi.org/10.1126/science.aal2418

Chen YS, Lu H, Liang J, Rosenthal A, Liu H, Sneddon G, McCarroll I, Zhao Z, Li W, Guo A & Cairney JM (2020). Observation of hydrogen trapping at dislocations, grain boundaries, and precipitates. *Science* **367**, 171–175. https://doi.org/10.1126/science.aaz0122

Choo WY & Lee JY (1982). Thermal analysis of trapped hydrogen in pure iron. *Metall Trans A* **13**, 135–140. https://doi.org/10.1007/BF02642424

Downloaded from https://academic.oup.com/mam/advance-article/doi/10.1093/mam/ozae081/7748435 by guest on 10 October 2024

Cuduvally R, Morris RJH, Oosterbos G, Ferrari P, Fleischmann C, Forbes RG & Vandervorst W (2022). Post-field ionization of Si clusters in atom probe tomography: A joint theoretical and experimental study. *J Appl Phys* **132**, 074901. https://doi.org/10.1063/5.0106692

Da Costa G, Vurpillot F, Bostel A, Bouet M & Deconihout B (2005). Design of a delay-line position-sensitive detector with improved performance. *Rev Sci Instrum* **76**, 13304. https://doi.org/10.1063/1.1829975

Dagan M, Hanna LR, Xu A, Roberts SG, Smith GDW, Gault B, Edmondson PD, Bagot PAJ & Moody MP (2015). Imaging of radiation damage using complementary field ion microscopy and atom probe tomography. *Ultramicroscopy* **159**, 387–394. https://doi.org/10.1016/j.ultramic.2015.02.017

Daly L, Lee MR, Bagot P, Halpin J, Smith W, Mcfadzean S, O'Brien AC, Griffin S, Hallis LJ & Cohen BE (2020). Exploring Mars at the nanoscale: Applications of transmission electron microscopy and atom probe tomography in planetary exploration. *IOP Conf Ser Mater Sci Eng* **891**, 012008. https://doi.org/10.1088/1757-899X/891/1/012008

Daly L, Lee MR, Darling JR, Mccarrol I, Yang L, Cairney J, Forman LV, Bland PA, Benedix GK, Fougerouse D, Rickard WDA, Saxey DW, Reddy SM, Smith W & Bagot PAJ (2021*a*). Developing atom probe tomography of phyllosilicates in preparation for extra-terrestrial sample return. *Geostand Geoanal Res* **45**, 427–441. https://doi.org/10.1111/ggr.12382

Daly L, Lee MR, Hallis LJ, Ishii HA, Bradley JP, Bland PA, Saxey DW, Fougerouse D, Rickard WDA, Forman LV, Timms NE, Jourdan F, Reddy SM, Salge T, Quadir Z, Christou E, Cox MA, Aguiar JA, Hattar K, Monterrosa A, Keller LP, Christoffersen R, Dukes CA, Loeffler MJ & Thompson MS (2021*b*). Solar wind contributions to Earth's oceans. *Nat Astron* **5**, 1275–1285. https://doi.org/10.1038/s41550-021-01487-w

de Graaf S, Momand J, Mitterbauer C, Lazar S & Kooi BJ (2020). Resolving hydrogen atoms at metal-metal hydride interfaces. *Sci Adv* **6**, eaay4312. https://doi.org/10.1126/sciadv.aay4312

DeRocher K, McLean M & Meisenkothen F (2022). A standards-based approach to dopant quantification using atom probe tomography. *Microsc Microanal* **28**, 728–729. https://doi.org/10.1017/S1431927622003373

Devaraj A, Mathews B, Arey B, Bagaasen L, Sevigny G & Senor D (2021). Neutron irradiation induced changes in isotopic abundance of 6Li and 3D nanoscale distribution of tritium in LiAlO2 pellets analyzed by atom probe tomography. *Mater Charact* **176**, 111095. https://doi.org/10.1016/j.matchar.2021.111095

Diercks DR, Gorman BP & Gerstl SSA (2017). An open-access atom probe tomography mass spectrum database. *Microsc Microanal* **23**, 664–665. https://doi.org/10.1017/S1431927617003981

Ding R & Jones IP (2011). In situ hydride formation in titanium during focused ion milling. *J Electron Microsc* **60**, 1–9. https://doi.org/10.1093/jmicro/dfq066

Djukic MB, Bakic GM, Sijacki Zeravcic V, Sedmak A & Rajicic B (2019). The synergistic action and interplay of hydrogen embrittlement mechanisms in steels and iron: Localized plasticity and decohesion. *Eng Fract Mech* **216**, 106528. https://doi.org/10.1016/j.engfracmech.2019.106528

Douglas JO, Conroy M, Giuliani F & Gault B (2023). In situ sputtering from the micromanipulator to enable cryogenic preparation of specimens for atom probe tomography by focused-ion beam. *Microsc Microanal* **29**, 1009–1017. https://doi.org/10.1093/micmic/ozad020

Dubochet J (2016). A reminiscence about early times of vitreous water in electron cryomicroscopy. *Biophys J* **110**, 756–757. https://doi.org/10.1016/j.bpj.2015.07.049

Dumpala S, Broderick SR, Bagot PAJ & Rajan K (2014). An integrated high temperature environmental cell for atom probe tomography studies of gas-surface reactions: Instrumentation and results. *Ultramicroscopy* **141**, 16–21. https://doi.org/10.1016/j.ultramic.2014.03.002

Eliezer D, Chakrapani DG, Altstetter CJ & Pugh EN (1979). The influence of austenite stability on the hydrogen embrittlement and stress-corrosion cracking of stainless steel. *Metall Trans A* **10**, 935–941. https://doi.org/10.1007/BF02658313

El-Zoka AA, Kim S-H, Deville S, Newman RC, Stephenson LT & Gault B (2020). Enabling near-atomic–scale analysis of frozen water. *Sci Adv* **6**, eabd6324. https://doi.org/10.1126/sciadv.abd6324

El-Zoka AA, Stephenson LT, Kim S-H, Gault B & Raabe D (2023). The fate of water in hydrogen-based iron oxide reduction. *Adv Sci* **10**, e2300626. https://doi.org/10.1002/advs.202300626

Evers S, Senöz C & Rohwerder M (2013). Hydrogen detection in metals: A review and introduction of a Kelvin probe approach. *Sci Technol Adv Mater* **14**, 014201. https://doi.org/10.1088/1468-6996/14/1/014201

Exertier F, La Fontaine A, Corcoran C, Piazolo S, Belousova E, Peng Z, Gault B, Saxey DW, Fougerouse D, Reddy SM, Pedrazzini S, Bagot PAJ, Moody MP, Langelier B, Moser DE, Botton GA, Vogel F, Thompson GB, Blanchard PT, Chiaramonti AN, Reinhard DA, Rice KP, Schreiber DK, Kruska K, Wang J & Cairney JM (2018). Atom probe tomography analysis of the reference zircon gj-1: An interlaboratory study. *Chem Geol* **495**, 27–35. https://doi.org/10.1016/j.chemgeo.2018.07.031

Felfer P, Ott B, Monajem M, Dalbauer V, Heller M, Josten J & Macaulay C (2022). An atom probe with ultra-low hydrogen background. *Microsc Microanal* **28**, 1255–1263. https://doi.org/10.1017/S1431927621013702

Felfer PJ, Alam T, Ringer SP & Cairney JM (2012). A reproducible method for damage-free site-specific preparation of atom probe tips from interfaces. *Microsc Res Tech* **75**, 484–491. https://doi.org/10.1002/jemt.21081

Forbes RG (1996). Field-ion imaging old and new. *Appl Surf Sci* **94–95**, 1–16. https://doi.org/10.1016/0169-4332(95)00516-1

Forbes RG (2008). Gas field ionization sources. In *Handbook of Charged Particle Optics*, Orloff J (Ed.), 2nd ed., pp. 87–128. Baton Roca: CRC Press.

Fromm E & Uchida H (1987). Surface phenomena in hydrogen absorption kinetics of metals and intermetallic compounds. *J Less Common Met* **131**, 1–12. https://doi.org/10.1016/0022-5088(87)90495-4

Gault B, Chiaramonti A, Cojocaru-Mirédin O, Stender P, Dubosq R, Freysoldt C, Makineni SK, Li T, Moody M & Cairney JM (2021). Atom probe tomography. *Nat Rev Methods Primers* **1**, 10.1038/s43586-021-00047-w. https://doi.org/10.1038/s43586-021-00047-w

Gault B, Khanchandani H, Prithiv TS, Antonov S & Britton TB (2023). Transmission Kikuchi diffraction mapping induces structural damage in atom probe specimens. *Microsc Microanal* **29**, 1026–1036. https://doi.org/10.1093/micmic/ozad029

Gault B, Saxey DW, Ashton MW, Sinnott SB, Chiaramonti AN, Moody MP & Schreiber DK (2016). Behavior of molecules and molecular ions near a field emitter. *New J Phys* **18**, 033031. https://doi.org/10.1088/1367-2630/18/3/033031

Gemma R, Al-Kassab T, Kirchheim R & Pundt A (2007). Studies on hydrogen loaded V–Fe8 at% films on Al2O3 substrate. *J Alloys Compd* **446–447**, 534–538. https://doi.org/10.1016/j.jallcom.2007.01.099

Gemma R, Al-Kassab T, Kirchheim R & Pundt A (2009). APT analyses of deuterium-loaded Fe/V multi-layered films. *Ultramicroscopy* **109**, 631–636. https://doi.org/10.1016/j.ultramic.2008.11.005

Gemma R, Al-Kassab T, Kirchheim R & Pundt A (2011). Analysis of deuterium in V–Fe5 at% film by atom probe tomography (APT). *J Alloys Compd* **509**, S872–S876. https://doi.org/10.1016/j.jallcom.2010.11.122

Gemma R, Al-Kassab T, Kirchheim R & Pundt A (2012). Visualization of deuterium dead layer by atom probe tomography. *Scr Mater* **67**, 903–906. https://doi.org/10.1016/j.scriptamat.2012.08.025

Gråsjö L, Hultquist G, Tan KL & Seo M (1995). Surface reactions on palladium hydride in vacuum, air and water studied in situ with mass spectrometry. *Appl Surf Sci* **89**, 21–34. https://doi.org/10.1016/0169-4332(95)00019-4

Greer J, Rout SS, Isheim D, Seidman DN, Wieler R & Heck PR (2020). Atom probe tomography of space-weathered lunar ilmenite grain

Downloaded from https://academic.oup.com/mam/advance-article/doi/10.1093/mam/ozae081/7748435 by guest on 10 October 2024

surfaces. *Meteorit Planet Sci* **55**, 426–440. https://doi.org/10.1111/maps.13443
Haley D, Bagot PAJ & Moody MP (2017). Atom probe analysis of Ex Situ Gas-charged stable hydrides. *Microsc Microanal* **23**, 307–313. https://doi.org/10.1017/S1431927616012769
Haley D, Merzlikin SV, Choi P & Raabe D (2014). Atom probe tomography observation of hydrogen in high-Mn steel and silver charged via an electrolytic route. *Int J Hydrogen Energy* **39**, 12221–12229. https://doi.org/10.1016/j.ijhydene.2014.05.169
Hamm M, Bongers MD, Roddatis V, Dietrich S, Lang K-H & Pundt A (2019). *In situ* observation of hydride nucleation and selective growth in magnesium thin-films with environmental transmission electron microscopy. *Int J Hydrogen Energy* **44**, 32112–32123. https://doi.org/10.1016/j.ijhydene.2019.10.057
Hanlon SM, Persaud SY, Long F, Korinek A & Daymond MR (2019). A solution to FIB induced artefact hydrides in Zr alloys. *J Nucl Mater* **515**, 122–134. https://doi.org/10.1016/j.jnucmat.2018.12.020
Hatzoglou C, Rouland S, Radiguet B, Etienne A, Costa GD, Sauvage X, Pareige P & Vurpillot F (2020). Preferential evaporation in atom probe tomography: An analytical approach. *Microsc Microanal* **26**, 689–698. https://doi.org/10.1017/S1431927620001749
Heck PR, Stadermann FJ, Isheim D, Auciello O, Daulton TL, Davis AM, Elam JW, Floss C, Hiller J, Larson DJ, Lewis JB, Mane A, Pellin MJ, Savina MR, Seidman DN & Stephan T (2014). Atom-probe analyses of nanodiamonds from allende. *Meteorit Planet Sci* **49**, 453–467. https://doi.org/10.1111/maps.12265
Henjered A & Norden H (1983). A controlled specimen preparation technique for interface studies with atom-probe field-ion microscopy. *J Phys E* **16**, 617–619. https://doi.org/10.1088/0022-3735/16/7/014
Herbig M & Kumar A (2021). Removal of hydrocarbon contamination and oxide films from atom probe specimens. *Microsc Res Tech* **84**, 291–297. https://doi.org/10.1002/jemt.23587
Hirth JP (1980). Effects of hydrogen on the properties of iron and steel. *Metall Trans A* **11**, 861–890. https://doi.org/10.1007/BF02654700
Hollenberg GW, Simonen EP, Kalinin G & Terlain A (1995). Tritium/hydrogen barrier development. *Fusion Eng Des* **28**, 190–208. https://doi.org/10.1016/0920-3796(94)00377-J
Holroyd NJH (1988). Environment-induced cracking of high-strength aluminum alloys. *Proceedings of Environment-Induced Cracking of Metals*. National association of Corrosion Engineers, Houston, TX. 311–345.
Hyde JM, Burke MG, Gault B, Saxey DW, Styman P, Wilford KB & Williams TJ (2011). Atom probe tomography of reactor pressure vessel steels: An analysis of data integrity. *Ultramicroscopy* **111**, 676–682. https://doi.org/10.1016/j.ultramic.2010.12.033
Jakob S, Sattari M, Sefer B, Ooi S & Thuvander M (2024). Characterization of hydrogen traps in a co-precipitation steel investigated by atom probe experiments without cryogenic transfer. *Scr Mater* **243**, 115963. https://doi.org/10.1016/j.scriptamat.2023.115963
Jenkins BM, Haley J, Chen L, Gault B, Burr PA, Callow A, Moody MP & Grovenor CRM (2023). Experimental and modelling evidence for hydrogen trapping at a β-Nb second phase particle and Nb-rich nanoclusters in neutron-irradiated low Sn ZIRLO. *J Nucl Mater* **587**, 154755. https://doi.org/10.1016/j.jnucmat.2023.154755
Jones C, Tuli V, Shah Z, Gass M, Burr PA, Preuss M & Moore KL (2021). Evidence of hydrogen trapping at second phase particles in zirconium alloys. *Sci Rep* **11**, 4370. https://doi.org/10.1038/s41598-021-83859-w
Jones ME, London AJ, Breen AJ, Styman PD, Sikotra S, Moody MP & Haley D (2022). Improving the quantification of deuterium in zirconium alloy atom probe tomography data using existing analysis methods. *Microsc Microanal* **28**, 1245–1254. https://doi.org/10.1017/S1431927621012848
Joseph S, Kontis P, Chang Y, Shi Y, Raabe D, Gault B & Dye D (2022). A cracking oxygen story: A new view of stress corrosion cracking in titanium alloys. *Acta Mater* **227**, 117687. https://doi.org/10.1016/j.actamat.2022.117687
Kellogg GL (1982). Measurement of the charge state distribution of field evaporated ions: Evidence for post-ionization. *Surf Sci* **120**, 319–333. https://doi.org/10.1016/0039-6028(82)90153-4
Kelly TF, Gribb TT, Olson JD, Martens RL, Shepard JD, Wiener SA, Kunicki TC, Ulfig RM, Lenz DR, Strennen EM, Oltman E, Bunton JH & Strait DR (2004). First data from a commercial local electrode atom probe (LEAP). *Microsc Microanal* **10**, 373–383. https://doi.org/10.1017/S1431927604040565
Kelly TF & Miller MK (2007). Invited review article: Atom probe tomography. *Rev Sci Instrum* **78**, 31101. https://doi.org/10.1063/1.2709758
Kesten P, Pundt A, Schmitz G, Weisheit M, Krebs HU & Kirchheim R (2002). H- and D distribution in metallic multilayers studied by 3-dimensional atom probe analysis and secondary ion mass spectrometry. *J Alloys Compd* **330–332**, 225–228. https://doi.org/10.1016/S0925-8388(01)01596-1
Khanchandani H, El-Zoka AA, Kim S-H, Tezins U, Vogel D, Sturm A, Raabe D, Gault B & Stephenson LT (2022*a*). Laser-equipped gas reaction chamber for probing environmentally sensitive materials at near atomic scale. *PLoS One* **17**, e0262543. https://doi.org/10.1371/journal.pone.0262543
Khanchandani H, Kim S-H, Varanasi RS, Prithiv T, Stephenson LT & Gault B (2022*b*). Hydrogen and deuterium charging of lifted-out specimens for atom probe tomography. *Open Res Eur* **1**, 122. https://doi.org/10.12688/openreseurope.14176.2
Khanchandani H, Rolli R, Schneider H-C, Kirchlechner C & Gault B (2023). Hydrogen embrittlement of twinning-induced plasticity steels: Contribution of segregation to twin boundaries. *Scr Mater* **225**, 115187. https://doi.org/10.1016/j.scriptamat.2022.115187
Kim SH, Antonov S, Zhou X, Stephenson LT, Jung C, El-Zoka AA, Schreiber DK, Conroy M & Gault B (2022). Atom probe analysis of electrode materials for Li-ion batteries: Challenges and ways forward. *J Mater Chem A Mater* **6**, 4883–5230. https://doi.org/10.1039/D1TA10050E
Kim S-H, Bhatt S, Schreiber DK, Neugebauer J, Freysoldt C, Gault B & Katnagallu S (2024). Understanding atom probe's analytical performance for iron oxides using correlation histograms and ab initio calculations. *New J Phys* **26**, 033021. https://doi.org/10.1088/1367-2630/ad309e
Kingham DR (1982). The post-ionization of field evaporated ions: A theoretical explanation of multiple charge states. *Surf Sci* **116**, 273–301. https://doi.org/10.1016/0039-6028(82)90434-4
Kolli RP (2017). Controlling residual hydrogen gas in mass spectra during pulsed laser atom probe tomography. *Adv Struct Chem Imaging* **3**, 10. https://doi.org/10.1186/s40679-017-0043-4
Kremer K, Schwarz-Selinger T & Jacob W (2021). Influence of thin tungsten oxide films on hydrogen isotope uptake and retention in tungsten—Evidence for permeation barrier effect. *Nucl Mater Energy* **27**, 100991. https://doi.org/10.1016/j.nme.2021.100991
Krishnaswamy SV & Müller EW (1977). Metal hydrides in pulsed field evaporation. *Zeitschrift für Physikalische Chemie* **104**, 121–130. https://doi.org/10.1524/zpch.1977.104.1-3.121
Larson DJ, Cerezo A, Juraszek J, Hono K & Schmitz G (2009). Atom-probe tomographic studies of thin films and multilayers. *MRS Bull* **34**, 732–737. https://doi.org/10.1557/mrs2009.247
Larson DJ, Foord DT, Petford-Long AK, Liew H, Blamire MG, Cerezo A & Smith GDW (1999). Field-ion specimen preparation using focused ion-beam milling. *Ultramicroscopy* **79**, 287–293. https://doi.org/10.1016/S0304-3991(99)00055-8
Li K, Aarholt T, Liu J, Hulme H, Garner A, Preuss M, Lozano-Perez S & Grovenor C (2019). 3D-characterization of deuterium distributions in zirconium oxide scale using high-resolution SIMS. *Appl Surf Sci* **464**, 311–320. https://doi.org/10.1016/j.apsusc.2018.09.101
Liu J, Taylor SD, Qafoku O, Arey BW, Colby R, Eaton A, Bartrand J, Shutthanandan V, Manandhar S & Perea DE (2022). Visualizing the distribution of water in nominally anhydrous minerals at the atomic scale: Insights from atom probe tomography on fayalite. *Geophys Res Lett* **49**, e2021GL094914. https://doi.org/10.1029/2021GL094914

Downloaded from https://academic.oup.com/mam/advance-article/doi/10.1093/mam/ozae081/7748435 by guest on 10 October 2024

Liu P-Y, Zhang B, Niu R, Lu S-L, Huang C, Wang M, Tian F, Mao Y, Li T, Burr PA, Lu H, Guo A, Yen H-W, Cairney JM, Chen H & Chen Y-S (2024). Engineering metal-carbide hydrogen traps in steels. *Nat Commun* **15**, 724. https://doi.org/10.1038/s41467-024-45017-4

López Freixes M, Zhou X, Zhao H, Godin H, Peguet L, Warner T & Gault B (2022). Revisiting stress-corrosion cracking and hydrogen embrittlement in 7xxx-Al alloys at the near-atomic-scale. *Nat Commun* **13**, 4290. https://doi.org/10.1038/s41467-022-31964-3

Lupu D, Radu Biriş A, Mişan I, Jianu A, Holzhüter G & Burkel E (2004). Hydrogen uptake by carbon nanofibers catalyzed by palladium. *Int J Hydrogen Energy* **29**, 97–102. https://doi.org/10.1016/S0360-3199(03)00055-7

Lynch S (2019). Discussion of some recent literature on hydrogen-embrittlement mechanisms: Addressing common misunderstandings. *Corros Rev* **37**, 377–395. https://doi.org/10.1515/corrrev-2019-0017

Maier H, Schwarz-Selinger T, Neu R, Garcia-Rosales C, Balden M, Calvo A, Dürbeck T, Manhard A, Ordás N & Silva TF (2019). Deuterium retention in tungsten based materials for fusion applications. *Nucl Mater Energy* **18**, 245–249. https://doi.org/10.1016/j.nme.2018.12.032

Mancini L, Amirifar N, Shinde D, Blum I, Gilbert M, Vella A, Vurpillot F, Lefebvre W, Lardé R, Talbot E, Pareige P, Portier X, Ziani A, Davesnne C, Durand C, Eymery J, Butté R, Carlin J-F, Grandjean N & Rigutti L (2014). Composition of wide bandgap semiconductor materials and nanostructures measured by atom probe tomography and its dependence on the surface electric field. *J Phys Chem C* **118**, 24136–24151. https://doi.org/10.1021/jp5071264

Marceau RKW, Choi P & Raabe D (2013). Understanding the detection of carbon in austenitic high-Mn steel using atom probe tomography. *Ultramicroscopy* **132**, 239–247. https://doi.org/10.1016/j.ultramic.2013.01.010

Marquis EA (2007). A reassessment of the metastable miscibility gap in Al-Ag alloys by atom probe tomography. *Microsc Microanal* **13**, 484–492. https://doi.org/10.1017/S1431927607070870

Martin TL, Coe C, Bagot PAJ, Morrall P, Smith GDW, Scott T & Moody MP (2016). Atomic-scale studies of uranium oxidation and corrosion by water vapour. *Sci Rep* **6**, 25618. https://doi.org/10.1038/srep25618

Martinka M (1981). Surface distributions of hydrogen field adsorbed on rhodium as displayed by imaging atom-probe. *Surf Sci* **109**, L539–L544. https://doi.org/10.1016/0039-6028(81)90418-0

Maxelon M, Pundt A, Pyckhout-Hintzen W, Barker J & Kirchheim R (2001). Interaction of hydrogen and deuterium with dislocations in palladium as observed by small angle neutron scattering. *Acta Mater* **49**, 2625–2634. https://doi.org/10.1016/S1359-6454(01)00185-9

Mayweg D, Eriksson J, Bäcke O, Breen AJ & Thuvander M (2023). Focused ion beam induced hydride formation does not affect Fe, Ni, Cr-clusters in irradiated Zircaloy-2. *J Nucl Mater* **581**, 154444. https://doi.org/10.1016/j.jnucmat.2023.154444

McCarroll IE, Bagot PAJ, Devaraj A, Perea DE & Cairney JM (2020). New frontiers in atom probe tomography: A review of research enabled by cryo and/or vacuum transfer systems. *Mater Today Adv* **7**, 100090. https://doi.org/10.1016/j.mtadv.2020.100090

McCarroll IE, Lin Y-C, Rosenthal A, Yen H-W & Cairney JM (2022). Hydrogen trapping at dislocations, carbides, copper precipitates and grain boundaries in a dual precipitating low-carbon martensitic steel. *Scr Mater* **221**, 114934. https://doi.org/10.1016/j.scriptamat.2022.114934

Meier MS, Bagot PAJ, Moody MP & Haley D (2023). Large-Scale atom probe tomography data mining: Methods and application to inform hydrogen behavior. *Microsc Microanal* **29**, 879–889. https://doi.org/10.1093/micmic/ozad027

Meier MS, Jones ME, Felfer PJ, Moody MP & Haley D (2022). Extending estimating hydrogen content in atom probe tomography experiments where H2 molecule formation occurs. *Microsc Microanal* **28**, 1231–1244. https://doi.org/10.1017/S1431927621012332

Meisenkothen F, Steel EB, Prosa TJ, Henry KT & Prakash Kolli R (2015). Effects of detector dead-time on quantitative analyses involving boron and multi-hit detection events in atom probe tomography. *Ultramicroscopy* **159 Pt 1**, 101–111. https://doi.org/10.1016/j.ultramic.2015.07.009

Merzlikin SV, Borodin S, Vogel D & Rohwerder M (2015). Ultra high vacuum high precision low background setup with temperature control for thermal desorption mass spectroscopy (TDA-MS) of hydrogen in metals. *Talanta* **136**, 108–113. https://doi.org/10.1016/j.talanta.2015.01.014

Miller MK & Hetherington MG (1991). Local magnification effects in the atom probe. *Surf Sci* **246**, 442–449. https://doi.org/10.1016/0039-6028(91)90449-3

Miller MK & Russell KF (2006). Atom probe specimen preparation with a dual beam SEM/FIB miller. *Ultramicroscopyvol* **107**, 761–766. https://doi.org/10.1016/j.ultramic.2007.02.023

Miller MK & Smith GDW (1981). An atom probe study of the anomalous field evaporation of alloys containing silicon. *J Vac Sci Technol B Nanotechnol Microelectron* **19**, 57–62. https://doi.org/10.1116/1.571017

Mouton I, Breen AJ, Wang S, Chang Y, Szczepaniak A, Kontis P, Stephenson LT, Raabe D, Herbig M, Britton TB & Gault B (2018). Quantification challenges for atom probe tomography of hydrogen and deuterium in Zircaloy-4. *Microsc Microanal* **25**, 481–488. https://doi.org/10.1017/S143192761801615X

Mouton I, Chang Y, Chakraborty P, Wang S, Stephenson LT, Ben Britton T & Gault B (2021). Hydride growth mechanism in zircaloy-4: Investigation of the partitioning of alloying elements. *Materialia* **15**, 101006. https://doi.org/10.1016/j.mtla.2021.101006

Müller EW & Bahadur K (1956). Field ionization of gases at a metal surface and the resolution of the field ion microscope. *Physical Rev* **102**, 624–631. https://doi.org/10.1103/PhysRev.102.624

Müller EW, Nakamura S, Nishikawa O & McLane SB (1965). Gas-Surface interactions and field-ion microscopy of nonrefractory metals. *J Appl Phys* **36**, 2496–2503. https://doi.org/10.1063/1.1714519

Müller M, Saxey DW, Smith GDW & Gault B (2011). Some aspects of the field evaporation behaviour of GaSb. *Ultramicroscopy* **111**, 487–492. https://doi.org/10.1016/j.ultramic.2010.11.019

Ott B, Heller M, Monajem M & Felfer P (2024). Miniaturized gas exposure devices for atom probe experiments. *Microsc Res Tech* **87**, 2113–2120. https://doi.org/10.1002/jemt.24573

Parvizi R, Hughes AE, Tan MY, Marceau RKW, Forsyth M, Cizek P & Glenn AM (2017). Probing corrosion initiation at interfacial nanostructures of AA2024-T3. *Corros Sci* **116**, 98–109. https://doi.org/10.1016/j.corsci.2016.12.006

Parvizi R, Marceau RKW, Hughes AE, Tan MY & Forsyth M (2014). Atom probe tomography study of the nanoscale heterostructure around an Al20Mn3Cu2 dispersoid in aluminum alloy 2024. *Langmuir* **30**, 14817–14823. https://doi.org/10.1021/la503418u

Peng Z, Vurpillot F, Choi P-P, Li Y, Raabe D & Gault B (2018). On the detection of multiple events in atom probe tomography. *Ultramicroscopy* **189**, 54–60. https://doi.org/10.1016/j.ultramic.2018.03.018

Perea DE, Gerstl SSA, Chin J, Hirschi B & Evans JE (2017). An environmental transfer hub for multimodal atom probe tomography. *Adv Struct Chem Imaging* **3**, 12. https://doi.org/10.1186/s40679-017-0045-2

Prosa TJ & Larson DJ (2017). Modern focused-ion-beam-based site-specific specimen preparation for atom probe tomography. *Microsc Microanal* **23**, 194–209. https://doi.org/10.1017/S1431927616012642

Prosa TJ, Strennen S, Olson D, Lawrence D & Larson DJ (2019). A study of parameters affecting atom probe specimen survivability. *Microsc Microanal* **25**, 425–437. https://doi.org/10.1017/S1431927618015258

Pundt A & Kirchheim R (2006). HYDROGEN IN METALS: Microstructural aspects. *Annu Rev Mater Res* **36**, 555–608. https://doi.org/10.1146/annurev.matsci.36.090804.094451

Rendulic KD & Knor Z (1967). Chemisorption and gas-promoted field evaporation. *Surf Sci* **7**, 205–214. https://doi.org/10.1016/0039-6028(67)90127-6

Downloaded from https://academic.oup.com/mam/advance-article/doi/10.1093/mam/ozae081/7748435 by guest on 10 October 2024

Robertson IM (2001). The effect of hydrogen on dislocation dynamics. *Eng Fract Mech* **68**, 671–692. https://doi.org/10.1016/S0013-7944(01)00011-X

Robertson IM, Sofronis P, Nagao A, Martin ML, Wang S, Gross DW & Nygren KE (2015). Hydrogen embrittlement understood. *Metall Mater Trans B* **46**, 1085–1103. https://doi.org/10.1007/s11663-015-0325-y

Rodrigues JA & Kirchheim R (1983). More evidence for the formation of a dense cottrell cloud of hydrogen (hydride) at dislocations in niobium and palladium. *Scripta Metallurgica* **17**, 159–164. https://doi.org/10.1016/0036-9748(83)90091-1

Rolander U & Andrén H-O (1989). Statistical correction for pile-up in the atom-probe detector system. *J Phys Colloques* **50**, C8-529–C8-534. https://doi.org/10.1051/jphyscol:1989891

Saksena A, Sun B, Dong X, Khanchandani H, Ponge D & Gault B (2023). Optimizing site-specific specimen preparation for atom probe tomography by using hydrogen for visualizing radiation-induced damage. *Int J Hydrogen Energy* **50**, 165–174. https://doi.org/10.1016/j.ijhydene.2023.09.057

Saxey DW (2011). Correlated ion analysis and the interpretation of atom probe mass spectra. *Ultramicroscopy* **111**, 473–479. https://doi.org/10.1016/j.ultramic.2010.11.021

Schreiber DK, Chiaramonti AN, Gordon LM & Kruska K (2014). Applicability of post-ionization theory to laser-assisted field evaporation of magnetite. *Appl Phys Lett* **105**, 244106. https://doi.org/10.1063/1.4904802

Schreiber DK, Perea DE, Ryan JV, Evans JE & Vienna JD (2018). A method for site-specific and cryogenic specimen fabrication of liquid/solid interfaces for atom probe tomography. *Ultramicroscopy* **194**, 89–99. https://doi.org/10.1016/j.ultramic.2018.07.010

Schwarz TM, Woods E, Singh MP, Chen X, Jung C, Aota LS, Jang K, Krämer M, Kim S-H, McCarroll I & Gault B (2024). In situ metallic coating of atom probe specimen for enhanced yield, performance, and increased field-of-view. *Microsc Microanal* ozae006. https://academic.oup.com/mam/advance-article/doi/10.1093/mam/ozae006/7608750

Seol JB, Kwak CM, Kim YT & Park CG (2016). Understanding of the field evaporation of surface modified oxide materials through transmission electron microscopy and atom probe tomography. *Appl Surf Sci* **368**, 368–377. https://doi.org/10.1016/j.apsusc.2016.01.196

Sha W, Chang L, Smith GDW, Liu C & Mittemeijer EJ (1992). Some aspects of atom-probe analysis of Fe-C and Fe-N systems. *Surf Sci* **266**, 416–423. https://doi.org/10.1016/0039-6028(92)91055-G

Shariq A, Mutas S, Wedderhoff K, Klein C, Hortenbach H, Teichert S, Kücher P & Gerstl SSA (2009). Investigations of field-evaporated end forms in voltage- and laser-pulsed atom probe tomography. *Ultramicroscopy* **109**, 472–479. https://doi.org/10.1016/j.ultramic.2008.10.001

Shi Y, Jones ME, Meier MS, Wright M, Polzin J-I, Kwapil W, Fischer C, Schubert MC, Grovenor C, Moody M & Bonilla RS (2022). Towards accurate atom scale characterisation of hydrogen passivation of interfaces in TOPCon architectures. *Sol Energy Mater Sol Cells* **246**, 111915. https://doi.org/10.1016/j.solmat.2022.111915

Simmons MY, Schofield SR, O'Brien JL, Curson NJ, Oberbeck L, Hallam T & Clark RG (2003). Towards the atomic-scale fabrication of a silicon-based solid state quantum computer. *Surf Sci* **532–535**, 1209–1218. https://doi.org/10.1016/S0039-6028(03)00485-0

Singh MP, Woods EV, Kim SH, Jung C, Aota LS & Gault B (2024). Facilitating the systematic nanoscale study of battery materials by atom probe tomography through in-situ metal coating. *Batteries Supercaps* **7**, e202300403. https://doi.org/10.1002/batt.202300403

Sofronis P & Robertson IM (2006). Viable mechanisms of hydrogen embrittlement—A review. *AIP Conf Proc* **837**, 64–70. https://doi.org/10.1063/1.2213060

Stephenson LT, Szczepaniak A, Mouton I, Rusitzka KAK, Breen AJ, Tezins U, Sturm A, Vogel D, Chang Y, Kontis P, Rosenthal A, Shepard JD, Maier U, Kelly TF, Raabe D & Gault B (2018). The Laplace project: An integrated suite for correlative atom probe tomography and electron microscopy under cryogenic and UHV conditions. *PLoS One* **13**, e0209211. https://doi.org/10.1371/journal.pone.0209211

Stepień ZM & Tsong TT (1998). Formation of metal hydride ions in low-temperature field evaporation. *Surf Sci* **409**, 57–68. https://doi.org/10.1016/S0039-6028(98)00200-3

Sun B, Lu W, Gault B, Ding R, Makineni SK, Wan D, Wu C-H, Chen H, Ponge D & Raabe D (2021). Chemical heterogeneity enhances hydrogen resistance in high-strength steels. *Nat Mater* **20**, 1629–1634. https://doi.org/10.1038/s41563-021-01050-y

Sundell G, Thuvander M & Andrén H-O (2013). Hydrogen analysis in APT: Methods to control adsorption and dissociation of H_2. *Ultramicroscopy* **132**, 285–289. https://doi.org/10.1016/j.ultramic.2013.01.007

Suzuki H & Takai K (2012). Summary of round-robin tests for standardizing hydrogen analysis procedures. *ISIJ Int* **52**, 174–180. https://doi.org/10.2355/isijinternational.52.174

Takahashi J, Kawakami K & Kobayashi Y (2018). Origin of hydrogen trapping site in vanadium carbide precipitation strengthening steel. *Acta Mater* **153**, 193–204. https://doi.org/10.1016/j.actamat.2018.05.003

Takahashi J, Kawakami K, Kobayashi Y & Tarui T (2010). The first direct observation of hydrogen trapping sites in TiC precipitation-hardening steel through atom probe tomography. *Scr Mater* **63**, 261–264. https://doi.org/10.1016/j.scriptamat.2010.03.012

Takahashi J, Kawakami K & Tarui T (2012). Direct observation of hydrogen-trapping sites in vanadium carbide precipitation steel by atom probe tomography. *Scr Mater* **67**, 213–216. https://doi.org/10.1016/j.scriptamat.2012.04.022

Thuvander M, Weidow J, Angseryd J, Falk LKL, Liu F, Sonestedt M, Stiller K & Andrén H-O (2011). Quantitative atom probe analysis of carbides. *Ultramicroscopy* **111**, 604–608. https://doi.org/10.1016/j.ultramic.2010.12.024

Tsong TT & Kellogg G (1975). Direct observation of directional walk of single adatoms and adatom polarizability. *Phys Rev B* **12**, 1343–1353. https://doi.org/10.1103/PhysRevB.12.1343

Tsong TT, Kinkus TJ & Ai CF (1983). Field induced and surface catalyzed formation of novel ions: A pulsed-laser time-of-flight atom-probe study. *J Chem Phys* **78**, 4763–4775. https://doi.org/10.1063/1.445276

Tweddle D, Hamer P, Shen Z, Markevich VP, Moody MP & Wilshaw PR (2019). Direct observation of hydrogen at defects in multicrystalline silicon. *Prog Photovoltaics Res Appl* **29**, 3184. https://doi.org/10.1002/pip.3184

Vurpillot F, Bostel A & Blavette D (2000). Trajectory overlaps and local magnification in three-dimensional atom probe. *Appl Phys Lett* **76**, 3127–3129. https://doi.org/10.1063/1.126545

Wada M, Uemori R & Nishikawa O (1983). Effect of hydrogen on the evaporation field of metals. *Surf Sci* **134**, 17–29. https://doi.org/10.1016/0039-6028(83)90309-6

Walck SD & Hren JJ (1984). FIM/IAP/TEM studies of hydrogen in metals. *Le J Phys Colloques* **45**, 355–360. https://doi.org/10.1051/jphyscol:1984959

Wang J, Toloczko MB, Kruska K, Schreiber DK, Edwards DJ, Zhu Z & Zhang J (2017). Carbon contamination during ion irradiation—Accurate detection and characterization of its effect on microstructure of ferritic/martensitic steels. *Sci Rep* **7**, 15813. https://doi.org/10.1038/s41598-017-15669-y

Wang S, Gavalda-Diaz O, Luo T, Guo L, Lovell E, Wilson N, Gault B, Ryan MP & Giuliani F (2022). The effect of hydrogen on the multiscale mechanical behaviour of a La(Fe, Mn, Si)13-based magnetocaloric material. *J Alloys Compd* **906**, 164274. https://doi.org/10.1016/j.jallcom.2022.164274

Wilkinson MD, Dumontier M, Aalbersberg IJ, Appleton G, Axton M, Baak A, Blomberg N, Boiten JW, da Silva Santos LB, Bourne PE, Bouwman J, Brookes AJ, Clark T, Crosas M, Dillo I, Dumon O, Edmunds S, Evelo CT, Finkers R, Gonzalez-Beltran A, Gray AJ, Groth P, Goble C, Grethe JS, Heringa J, 't Hoen PA, Hooft R, Kuhn T, Kok R, Kok J, Lusher SJ, Martone ME, Mons A, Packer AL, Persson B, Rocca-Serra P, Roos M, van Schaik R, Sansone SA, Schultes E, Sengstag T, Slater T, Strawn G, Swertz MA, Thompson M, van der Lei J, van Mulligen E, Velterop J, Waagmeester A,

Downloaded from https://academic.oup.com/mam/advance-article/doi/10.1093/mam/ozae081/7748435 by guest on 10 October 2024

Wittenburg P, Wolstencroft K, Zhao J & Mons B (2016). The FAIR guiding principles for scientific data management and stewardship. *Sci Data* **3**, 160018. https://doi.org/10.1038/sdata.2016.18

Woods EV, Singh MP, Kim S-H, Schwarz TM, Douglas JO, El-Zoka AA, Giulani F & Gault B (2023). A versatile and reproducible cryo-sample preparation methodology for atom probe studies. *Microsc Microanal* **29**, 1992–2003. https://doi.org/10.1093/micmic/ozad120

Xu H, Li Z, He F, Wang X, Atia-Tul-Noor A, Kielpinski D, Sang RT & Litvinyuk IV (2017). Observing electron localization in a dissociating H2+ molecule in real time. *Nat Commun* **8**, 15849. https://doi.org/10.1038/ncomms15849

Yan F, Mouton I, Stephenson LT, Breen AJ, Chang Y, Ponge D, Raabe D & Gault B (2019). Atomic-scale investigation of hydrogen distribution in a Ti–Mo alloy. *Scr Mater* **162**, 321–325. https://doi.org/10.1016/j.scriptamat.2018.11.040

Yoo S-H, Kim S-H, Woods E, Gault B, Todorova M & Neugebauer J (2022). Origins of the hydrogen signal in atom probe tomography: Case studies of alkali and noble metals. *New J Phys* **24**, 013008. https://doi.org/10.1088/1367-2630/ac40cd

Zanuttini D, Blum I, Di Russo E, Rigutti L, Vurpillot F, Douady J, Jacquet E, Anglade PM & Gervais B (2018). Dissociation of GaN2+ and AlN2+ in APT: Analysis of experimental measurements. *J Chem Phys* **149**, 134311. https://doi.org/10.1063/1.5037010

Zanuttini D, Blum I, Rigutti L, Vurpillot F, Douady J, Jacquet E, Anglade P-M & Gervais B (2017). Simulation of field-induced molecular dissociation in atom-probe tomography: Identification of a neutral emission channel. *Phys Rev A* **95**, 61401. https://doi.org/10.1103/PhysRevA.95.061401

Zhang S, Gervinskas G, Liu Y, Marceau RKW & Fu J (2021). Nanoscale coating on tip geometry by cryogenic focused ion beam deposition. *Appl Surf Sci* **564**, 150355. https://doi.org/10.1016/j.apsusc.2021.150355

Zhao H, Chakraborty P, Ponge D, Hickel T, Sun B, Wu C-H, Gault B & Raabe D (2022). Hydrogen trapping and embrittlement in high-strength Al-alloys. *Nature* **602**, 437–441. https://doi.org/10.1038/s41586-021-04343-z

Zhao H, Yin Y, Wu Y, Zhang S, Mingers AM, Ponge D, Gault B, Rohwerder M & Raabe D (2024). How solute atoms control aqueous corrosion of Al-alloys. *Nat Commun* **15**, 561. https://doi.org/10.1038/s41467-024-44802-5

Ziegler JF & Biersack JP (1985). The stopping and range of ions in matter. In *Treatise on Heavy-Ion Science*, Bromley DA (Eds.), pp. 93–129. Boston, MA: Springer.

Downloaded from https://academic.oup.com/mam/advance-article/doi/10.1093/mam/ozae081/7748435 by guest on 10 October 2024

TESCAN
PERFORMANCE IN NANOSPACE

TESCAN AMBER X 2

PLASMA FIB-SEM REDEFINED

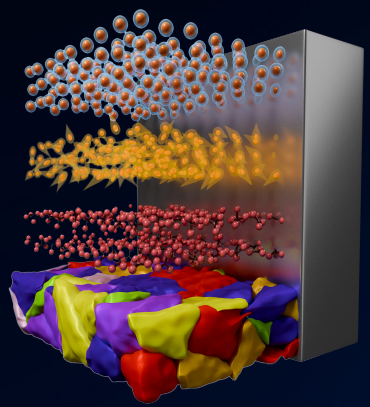

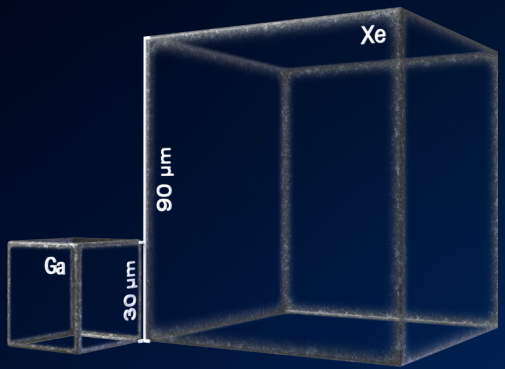

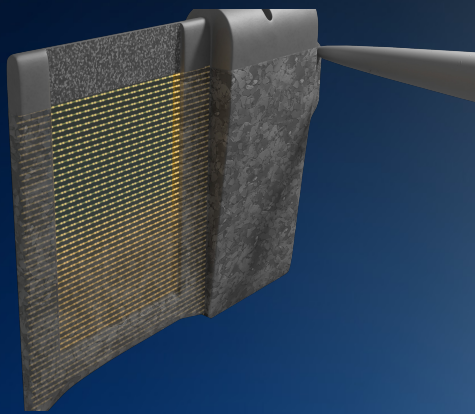

UTILITY REDEFINED

SPEED REDEFINED

PRECISION REDEFINED

info.tescan.com